



Analysis of Rock Quarry Sand and Bottom Ash Reinforced by Randomly Distributed PET Rings

Jakub Stacho ^{1*}, Ivan Slávik ¹, Monika Sulovska ¹, Matus Kolenak ¹

¹ Department of Geotechnics, Faculty of Civil Engineering, Slovak University of Technology in Bratislava, Bratislava 810 05, Slovakia.

Received 16 January 2025; Revised 23 April 2025; Accepted 28 April 2025; Published 01 May 2025

Abstract

The study presented deals with determining the shear strength and deformation properties of coarse-grained waste materials, such as rock quarry sand (RQS) and bottom ash (BA), which can be improved using randomly distributed reinforcements made of polyethylene terephthalate (PET) rings. The tests were executed for a degree of reinforcement n , i.e., a ratio of a PET ring weight to the weight of the dry parent materials, which equals about $n = 0.25\%$, 0.5% , and 1.0% in the case of RQS, and $n = 0.5\%$, 1.0% , and 1.5% in the case of BA. The results showed that the most effective improvement in the shear strength properties can be achieved for $n = 0.25 - 0.5\%$ in the case of RQS and $n = 0.5 - 1.0\%$ in the case of BA. Reinforcing RQS by $n = 1.0\%$ or BA by $n = 1.5\%$ led to a significant decrease in the 1D deformation modulus. The positive effect of randomly distributed PET ring reinforcements on the properties of RQS and BA materials was also demonstrated using physical modeling. An embankment model made of RQS and reinforced by PET rings ($n = 0.25\%$) can carry up to a 2.8 times greater load than an embankment model made of the parent RQS. An embankment model made of BA with PET rings ($n = 0.5\%$) can carry up to a 2.3 times greater load than an embankment model made of the parent BA.

Keywords: Soil Improvement; Soil Reinforcement; Distributed Reinforcement; PET; PET Rings; Rock Quarry Sand; Bottom Ash; Direct Shear Test; Compression Test; Physical Modeling.

1. Introduction

In recent years, when designing buildings and civil engineering structures, more and more emphasis has been placed on sustainable development or reducing environmental burdens, minimizing greenhouse gas emissions, and reducing carbon footprints. This trend can also be seen in geotechnical engineering, where there is an effort to replace conventional materials and technologies with "alternative" materials and technologies that are more economical and eco-friendly. Typical examples are earth structures reinforced with geosynthetics, which have been proposed since the 1980s. These structures are, for example, block-faced geogrid-reinforced earth structures [1, 2], wrapped geogrid-reinforced earth structures [3-5], and reinforced railway embankments [6-8], or reinforced road embankments [9-11]. The embankments can also be founded on the geogrid-reinforced foundation supported by deep soil mixing columns [12], or piles [13]. It has not been easy to summarize the results of all previous researchers because these technologies are constantly being developed and used worldwide. These constructions can be considered ecological, but in most cases, they are made of coarse-grained natural materials [1-4, 10], which need to be mined. Gravel pits or surface quarries are thus created, which have a significant impact on the environment. These issues have inspired researchers to replace conventional materials with alternative materials that are not commonly used in the construction of geotechnical structures, such as embankments. In the study presented, two typical waste materials have been considered, i.e., rock

* Corresponding author: jakub.stacho@stuba.sk

<http://dx.doi.org/10.28991/CEJ-2025-011-05-06>



© 2025 by the authors. Licensee C.E.J, Tehran, Iran. This article is an open access article distributed under the terms and conditions of the Creative Commons Attribution (CC-BY) license (<http://creativecommons.org/licenses/by/4.0/>).

quarry sand (RQS), which is produced in large quantities as waste from surface mining activities (Figure 1-a), and bottom ash (BA), which arises as waste from thermal power plant energy production (Figure 1-b). It was necessary to investigate non-traditional and alternative reinforcement methods, which are not typically used in practice, to improve the mechanical properties of these waste materials.



Figure 1. View of the sampling location: (a) Rock Quarry Sand (RQS), (b) Bottom ash (BA)

Over the last 40 years, many researchers have investigated the improvement of low-bearing soils and waste materials using different natural or artificial reinforcing materials [14]. Researchers most often examine the impact of distributed reinforcements on the improvement of the properties of fly ash (FA) [15, 16], bottom ash (BA) [17], volcanic ash (VA) [18], black cotton soil (BCS) [19], rock quarry dust (RQD) [20], clay (C) [21], sand-clay (SC) [22], expansive soil [23-26], sand [27-30], medium sand [17, 29, 31], or coarse sand [32-34]. These materials can be successfully improved using distributed reinforcement made of polyester fibers [15, 18, 24, 28, 35], low-density polyethylene sheets [27], weak paper fibers [36], bagasse fibers [25], coir fibers [26], corn-silk fibers [37], nylon fibers [33, 38], glass fibers [21], polymer tire fibers [21], micro-synthetic fibers [29], treated Kenaf fiber bundles [22], carbon fiber polymer [30], jute fibers [23, 39, 40], polyethylene terephthalate (PET) fibers [31, 32, 41], polypropylene fibers [17, 42-44], PET strips [41, 45-47], PET flakes [48], PET chips [49], or waste tire textile fibers [34, 50]. Some researchers have also focused on improving soil or ash using PET reinforcements (rings from PET bottles) connected to create a cellular reinforcement [20, 51].

The effect of distributed reinforcement on improving the shear strength properties of materials, such as, e.g., sand or ash, can be significant. Compared to the parent (unreinforced) sand, the shear strength of sand reinforced by a 1 % amount of nylon fibers can increase by about 37 % [33]. In the case of sand reinforced by PET fibers, an increase in the shear strength of about 39% can be achieved [32]. Festugato et al. [28] have found improvement in the angle of the shear strength of sand reinforced by polypropylene fibers by about 1.34 times in a drained condition and 1.18 times in an undrained condition. They have also reported significant improvement in undrained cohesion. Using kenaf fiber bundles also can improve the cohesion of a sand-clay mixture by about 15% and the angle of the shear strength by about 13% [22]. Moreover, the shear strength of fiber-reinforced expansive soil can be significantly improved, i.e., a 1.4-times increase in the cohesion and a 1.44-times increase in the angle of the shear strength can be achieved [25]. The shear strength of the materials tested using different types of distributed reinforcement can be improved in static and dynamic or cyclic loadings [28, 34, 52]. Many researchers have used the triaxial tests in their studies to determine the improvement in shear strength [20, 25, 27-29, 31, 32, 34, 36, 51]. Other researchers preferred the direct shear test [21,

30, 33, 50]. A large-size direct shear test can represent one of the best options in determining the shear strength of the material reinforced [16, 22, 53, 54], mainly when relatively large-length fibers are used as randomly distributed reinforcement.

In most cases, existing studies have focused on determining the optimal amount of the type of distributed reinforcement to improve the shear strength properties of the material tested. The degree of reinforcement usually ranges up to 2 %, where the positive effect of the reinforcement can be expected to improve the shear strength properties of the materials tested [21, 27, 33, 50]. The optimum degree of reinforcement depends on the material and the type of reinforcement (material, shape, and size). In the case of sand reinforced by PET fibers, the optimum degree of reinforcement is usually below 0.75 % [25].

Physical modeling can also play an essential role in investigating the effect of the different types of reinforcement on the shear strength of the material tested [55-57]. Khan et al. [56] presented the results of a retaining wall in which a shredded tire sand mixture was used as a backfill material. In the case of this reinforced backfill, they reported that at stresses higher than 20 kPa, a significant reduction in horizontal deformations occurred. However, they also noted a slight increase in the vertical deformations for the retaining wall with the reinforced backfill. They attributed the increase in the vertical deformations to the shredded tire in the sand being more compressible than sand grains. As a reinforcement material, the PET rings were analyzed by Lal & Mandal [58], and Nadaf & Mandal [59]. In both studies, the PET rings were connected to each other, creating a cellular reinforcement. They presented all the results in the relative deformations, which permitted an improved interpretation for further practical solutions. A fly ash material reinforced by PET rings in the form of cellular reinforcement significantly reduces deformations of a reinforced retaining wall [58] and a reinforced embankment [59].

The studies mentioned above clearly show that researchers mainly focus on utilizing the type of waste material that is in excess. The statistics show that a total of 5 million tons of PET materials were found on the European market in 2022. About 2.8 million tons of PET bottles were collected and used for recycling [60]. Although that amounts to almost 60%, which could be considered a high number, around 40 % of PET bottles produced are not recycled and thus create waste that could eventually be used as a distributed reinforcement for non-standard construction or fill materials. The PET material has been analyzed as a reinforcing material so far only in the form of fibers [31, 32], flakes, strips, chips [49], or PET rings, where rings were connected using plastic tapes [20, 51, 58, 59, 61, 62]. The PET rings connected to each other can improve the strength and stability of a reinforced earth structure; however, the manual connection of the cut PET bottles is very laborious, and it remains questionable whether it would be taken in practice. In contrast to the studies, randomly distributed PET rings were used as the reinforcement material in the analysis presented. This has led the authors to the idea of using the PET ring as a randomly distributed reinforcement, which has not been investigated yet. The submitted study focused on determining the optimal amount of PET rings to improve the strength and deformation properties of RQS and BA materials. The shear strength properties were determined using a large-size direct shear test apparatus, and the deformation properties were tested using a large-sized 1D compression test. The results obtained from the laboratory tests were further verified using physical modeling. The basic work process is schematically shown in Figure 2.

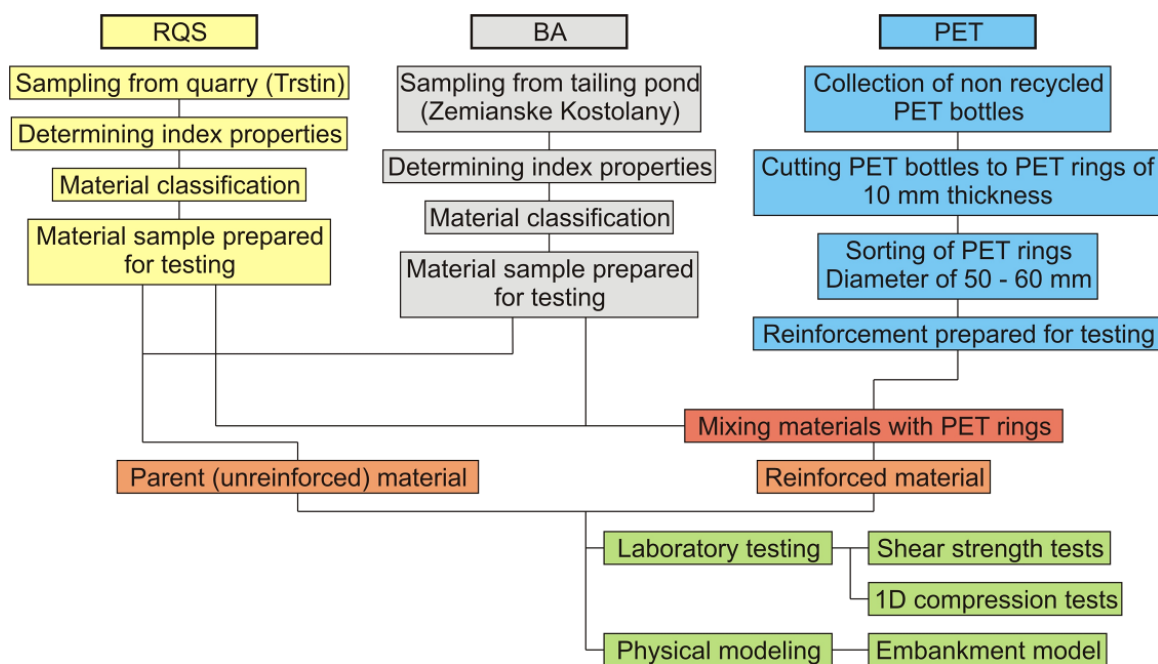


Figure 2. A basic work process

2. Properties of the Materials Tested

Both materials used in the study, i.e., RQS and BA, are considered to be waste materials. BA material, which is created as a by-product of coal combustion in the Novaky thermal power plant (Slovakia), was taken from the definitive tailings pond in Zemianske Kostolany (Slovakia). The RQS material was created as a by-product in an active quarry in the village of Trstin, which is located in the Small Carpathians region (Slovakia). The exact sampling locations are drawn in Figure 3 (More detailed views are presented in Figure 1).

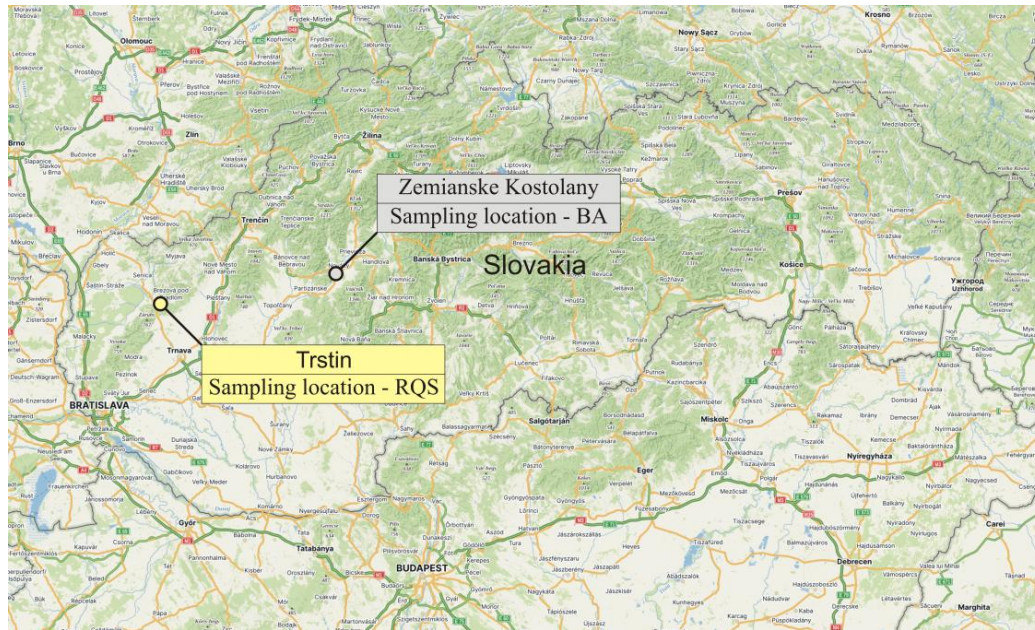


Figure 3. Sampling locations plotted on the map of Slovakia

The grain-size distribution curves (Figure 4) were determined according to the STN EN ISO 17892-4:2023 standard (Laboratory testing of soil: Part 4-Determination of particle size distribution). The grain size distributions of the samples were determined using approximately 5 kg of the dried sample. According to the STN 72 1001:2010 standard (Classification of soil and rock), RQS material can be classified as poorly graded sand (SP), and BA material can be classified as sand with a fine content (S-F). The index properties and the shear strength properties of both materials were determined concerning the STN EN ISO 17892-2:2023 standard (Laboratory testing of soil: Part 2-Determination of bulk density) and the STN EN ISO 17892-10:2023 standard (Laboratory testing of soil: Part 10-Direct shear test). The bulk densities, which were determined using a container with a volume of 5930 cm³, were repeated three times to minimize any errors from the testing procedure. The shear strength properties were determined using a SHEARMATIC 27-WF 2304 large-size direct shear test apparatus. The authors previously presented the testing procedure for the parent coarse-grained material [63]. The index and shear strength properties are summarized in Table 1.

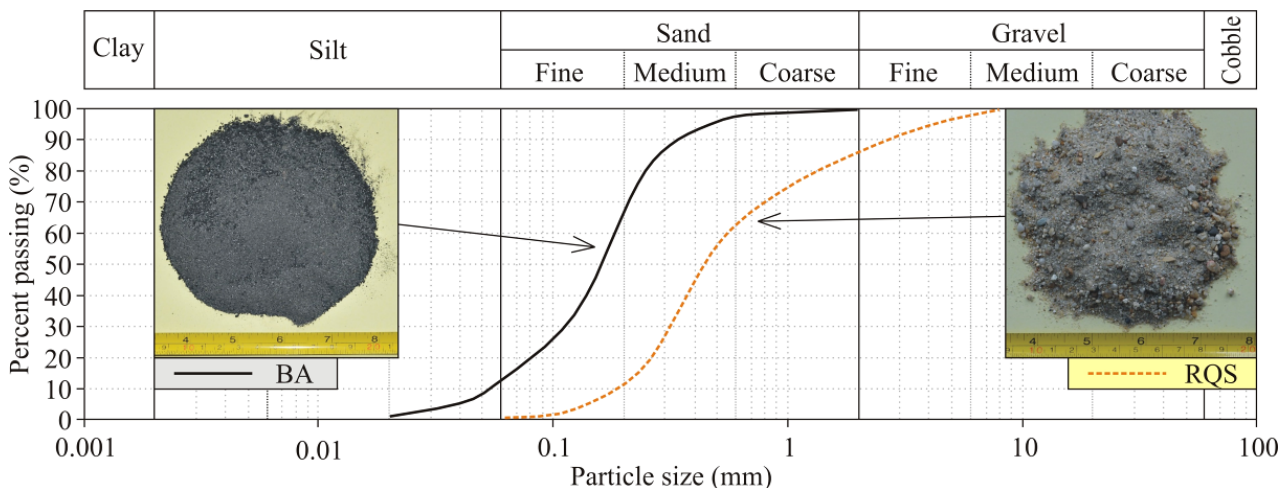


Figure 4. Grain-size distribution curves of the materials tested

Table 1. Index properties and the shear strength properties of the materials tested

	Parameter	Symbol (Unit)	Material	
			RQS	BA
The index properties	The minimum dry bulk density	$\rho_{\min,d}$ (kg.m ⁻³)	1448.1	784.5
	The maximum dry bulk density	$\rho_{\max,d}$ (kg.m ⁻³)	1751.1	1079.4
	The solid particle density	ρ_s (kg.m ⁻³)	2511.8	2020.0
	The coefficient of the uniformity	C_u (-)	3.38	3.50
	The coefficient of the curvature	C_c (-)	0.98	1.19
The shear strength properties (drained)	The peak angle of the shear strength	ϕ' (°)	34.14	37.26
	The apparent peak cohesion	c' (kPa)	0	1.52
	The critical angle of the shear strength	ϕ'_c (°)	30.30	35.80
	The apparent critical cohesion	c'_c (kPa)	0	0

The PET rings used as randomly distributed reinforcement material in this study were made from 0.5-liter PET bottles. They were collected in a bin for PET bottles, which were not used for recycling. The PET rings had a diameter of 50-60 mm and a thickness of 10 mm. These PET rings were cut from PET bottles using a professional cutter. The bottlenecks (the smaller diameter parts) were omitted from the presented study. The PET rings can also be seen as reinforcing material in Figure 5.

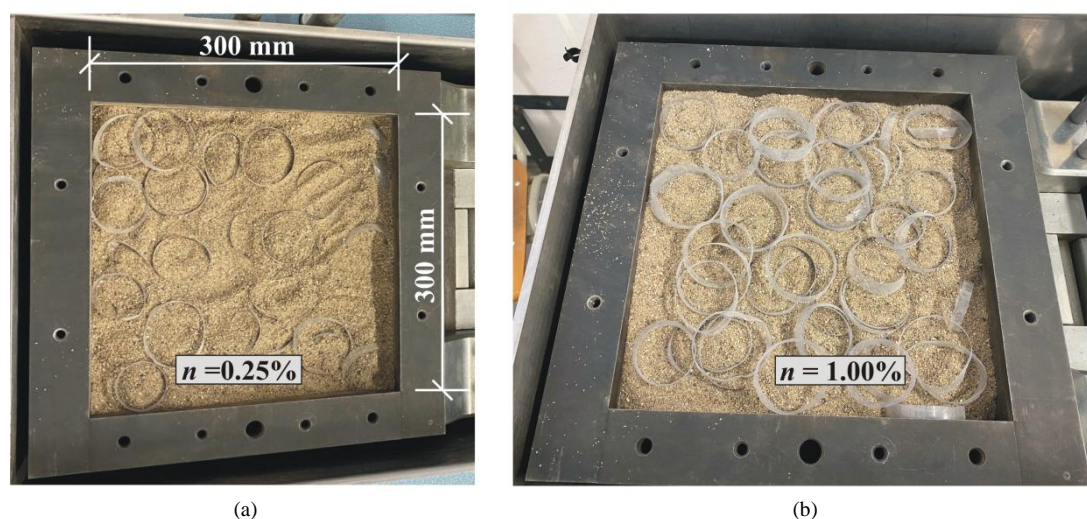


Figure 5. View of the shear box: RQS reinforced by PET rings: (a) $n = 0.25\%$ and (b) $n = 1.0\%$

3. Preparation and Procedure of the Laboratory Testing and the Physical Modeling

The laboratory tests were carried out in the first step of the testing. The aim was to determine the shear strength and deformation parameters of the reinforced materials and to determine the optimal degree of reinforcement for both materials, RQS and BA.

3.1. Laboratory Testing using a Large-Size Direct Shear Test Apparatus

The laboratory tests were done using a SHEARMATIC 27-WF 2304 large-sized, displacement-controlled shear strength apparatus. The dimensions of the shear box used were equal to $300 \times 300 \times 200$ mm (width \times length \times height). In the beginning, the boundary conditions, which were observed for all the tests performed, were established. In the first step, the sample was compacted in the shear box. The compaction took place on three levels using a rubber hammer. A total of 20 kg of RQS or 13 kg of BA was used. Subsequently, the density index I_D was determined, which served as a control for achieving the same degree of compaction.

The shear strength tests were divided into two main phases, i.e., the consolidation phase and the shear strength phase. The tests were done for three normal stresses, i.e., $\sigma' = 18, 42,$ and 92 kPa. In such a range of normal stress, there is no damage to the distributed reinforcement. The consolidation phase took about 240 minutes, sufficiently ensuring steady deformations before the shear tests. The horizontal movement applied in the second testing phase was equal to 0.2 mm/min. The maximum horizontal movement was about 60 mm, corresponding to a horizontal strain ε_h of about 20%. The tests were fully automated, and the digital recording contained normal and shear stresses as well as horizontal and

vertical deformations. The first series of tests was executed on parent (unreinforced) materials. The shear strength test results have already been presented in Table 1. Subsequently, the RQS and BA parent materials were reinforced with PET rings (created by cutting non-recycled 0.5 liter PET bottles with a diameter of about 50-60 mm and a thickness of about 10 mm). A separate container was used for mixing the parent material and PET rings (the homogeneous mixing was only checked visually). A degree of reinforcement n was determined using the following formula:

$$n = \frac{m_r}{m} \quad (1)$$

where m_r is the weight of the PET rings, and m is the dry weight of the parent material.

In the case of RQS, the shear strength tests were performed for $n = 0.25, 0.5, \text{ and } 1.0 \%$. A higher degree of reinforcement proved problematic in creating a homogeneous reinforced material sample, i.e., there were too many PET rings. Because of its lower bulk density, in the case of BA, the degree of reinforcement n was selected at the values of 0.5, 1.0, and 1.5 %. Other authors have also noted the degree of reinforcement in the same way [15, 21, 22, 24, 25, 28, 29, 31, 33, 35, 49, 50, 53, 54]. The degree of reinforcement could also be stated as a ratio of the volume of the reinforcement material to the volume of the parent material, as stated by Li & Zornberg [36]; however, from a practical point of view, it is not used. Table 2 shows the degrees of reinforcement applied that express the weight ratios and the corresponding degrees of reinforcement that express the volume ratios.

Table 2. The degree of reinforcement applied in the study

Material	The degree of reinforcement	n (%)		
RQS	dry weight of reinforced material / dry weight of parent material	0.25	0.50	1.00
	volume of reinforced material / volume of parent material	0.289	0.579	1.157
BA	dry weight of reinforced material / dry weight of parent material	0.50	1.00	1.50
	volume of reinforced material / volume of parent material	0.377	0.734	1.067

An example of reinforcing the RQS material with the PET rings is shown in Figure 5. The shear strength properties of the materials reinforced by PET rings, namely, the effective angle of the shear strength φ'_r and the effective apparent cohesion c'_r , were determined in the same way as for the parent materials, using Equations 2 and 3. The dilatancy angle was determined according to Equation 4, which is the most common method applied for its evaluation from the direct shear test results [64, 65]:

$$\tan \varphi' = \frac{1}{s \sum (\sigma')^2 - (\sum \sigma')^2} \cdot (s \sum \tau' \sigma' - \sum \tau' \sum \sigma') \quad (2)$$

$$c' = \frac{1}{s \sum (\sigma')^2 - (\sum \sigma')^2} \cdot (\sum \tau' \sum (\sigma')^2 - \sum \sigma' \sum \tau' \sigma') \quad (3)$$

$$\tan \psi' = -\frac{d\varepsilon_{yy}}{d\gamma_{yx}} = \frac{d_v}{d_u} \quad (4)$$

where s is the number of specimens; σ' and τ' are the normal and shear stresses, and ε_{yy} and γ_{yx} are the vertical compressive and shear strains, while d_v and d_u represent the vertical deformation and the shear displacement.

The first phases of the shear tests, i.e., the consolidation phases, were used to plot the compression curves. This allowed for determining the deformation behavior of the parent as well as the reinforced materials. The results of the test were evaluated according to the procedure for the oedometer tests, but the evaluation has been presented as for an axial compressibility test represented by an E_{1D} parameter instead of an E_{oed} parameter since the size of the shear box was not in accordance with the requirement of the STN EN ISO 17892-5:2023 standard (Laboratory testing of soil: Part 5 - Incremental loading oedometer test). This evaluation was sufficient to observe differences in the deformation behavior between the parent materials and those reinforced by PET rings. The E_{1D} parameter was determined according to Equation 5 for three loading steps, i.e., $\sigma' = 0 - 18, 18 - 42, \text{ and } 42 - 92$ kPa; where σ'_i is the normal stress, and ε_i is the vertical strain.

$$E_{1D,i} = \frac{\sigma'_i - \sigma'_{i-1}}{\varepsilon_i - \varepsilon_{i-1}} \quad (5)$$

3.2. Testing using a Physical Model

A physical model was built to verify the results of the laboratory testing. A large testing box (container) was created for the physical model, the dimensions of which were inspired by the study presented by Won et al. [66]. The dimensions of the testing box were as follows: length = 2.0 m, width = 0.5 m, and height = 1.0 m (Figure 6). The main frame of the box was made of U80 steel profiles and RHS50/30/5 steel profile bracing ribs. The front wall was made of 10 mm thick

Plexiglas, and the other walls were made of 2 mm thick sheet metal. The dimensions of the box permitted the creation of a half part of an embankment model with a height of 600 mm, a width of 800 mm at the top, and a width of about 1550 mm at the bottom. The embankment slope was about 1:1.25 (Figure 6). These dimensions were applied in all the models tested. The vertical load from a hydraulic piston was applied through a steel plate with dimensions of 300 x 300 x 10 mm (length x width x thickness). The vertical deformation of the loading plate was measured using a couple of analog deformation sensors. The horizontal deformation of the slope was measured using digital LVDT sensors placed at five different heights, i.e., 100 mm, 200 mm, 300 mm, 400 mm, and 500 mm from the bottom. The rods of LVDT sensors were fixed with the embankment body using plastic plates embedded about 30 mm into the testing material. The internal deformation of the body of the embankment was recorded in the following way:

- A 100 × 100 mm mesh was plotted on the Plexiglas wall of the model;
- Targets were placed on the side of the embankment's body, see Figure 6 (also, the geometry of the target is plotted in Figure 6);
- The test was recorded in a 4K resolution using a fixed camera;
- The digital sequences were transferred into Corel DRAW graphic software, which made it possible to determine the amount of displacement of the individual targets.

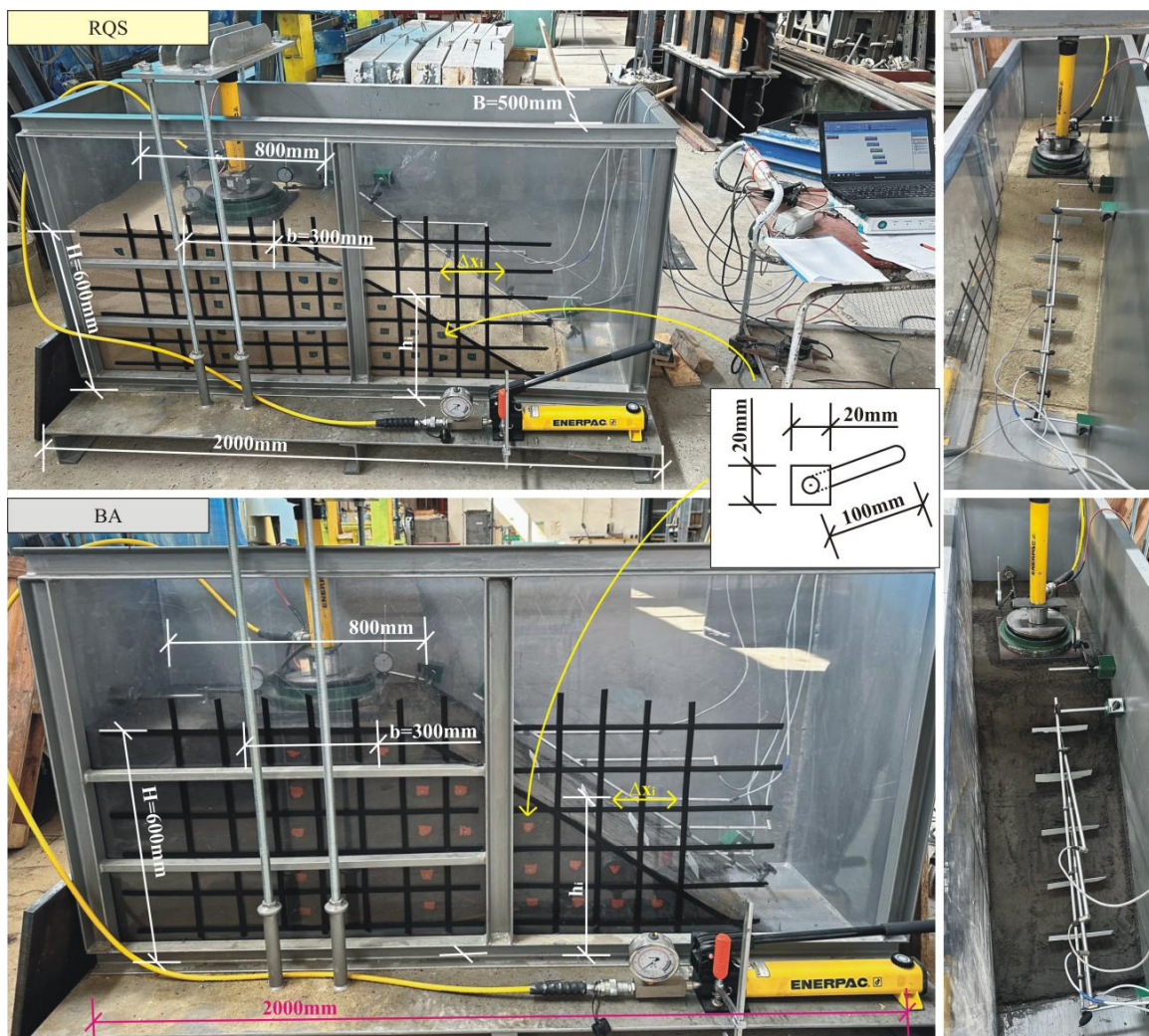


Figure 6. View of the geometry and instrumentation of the physical model

The embankment body was gradually built into 10 cm thick layers, which were compacted using a rubber hammer to achieve approximately the same degree of compaction as in the laboratory tests. In the first step, the tests were executed for the embankment models made of the parent materials. In the second step, the tests were executed for the materials reinforced by PET rings. Only the lowest degree of reinforcement was tested, i.e., $n = 0.25\%$ for the embankment model made of RQS and $n = 0.50\%$ for the embankment model made of BA. This was considered sufficient to demonstrate the effectiveness of the PET ring reinforcement on the embankment models' behavior. The results of the physical modeling were presented in relative values [58, 59].

4. Results of the study

4.1. Evaluation of the Laboratory Tests

The reinforcement of RQS and BA with PET rings only had a negligible effect on the material's bulk density change. As the volumetric weight of PET material was approximately 1350 kg.m^{-3} and made up a maximum of 1.0 % of the weight of the RQS sample or 1.5 % of the weight of the BA sample, changes in the bulk density were very small. Due to the scope, they are not mentioned in the paper, as they were evaluated as insignificant. The laboratory tests were, therefore, primarily aimed at determining the impact of the PET rings on the shear strength and deformation properties of the materials tested.

4.1.1. Shear Strength Properties of RQS and BA Reinforced by PET Rings

The shear strength curves of the parent materials and the materials reinforced by the PET rings in the different degrees of reinforcement determined by the large-size direct shear test are plotted in Figure 7 for $\sigma' = 18 \text{ kPa}$, Figure 8 for $\sigma' = 42 \text{ kPa}$, and Figure 9 for $\sigma' = 92 \text{ kPa}$. The density indexes I_D of the materials tested were about $I_D = 0.7 - 0.75$ for RQS and $I_D = 0.65 - 0.70$ for BA.

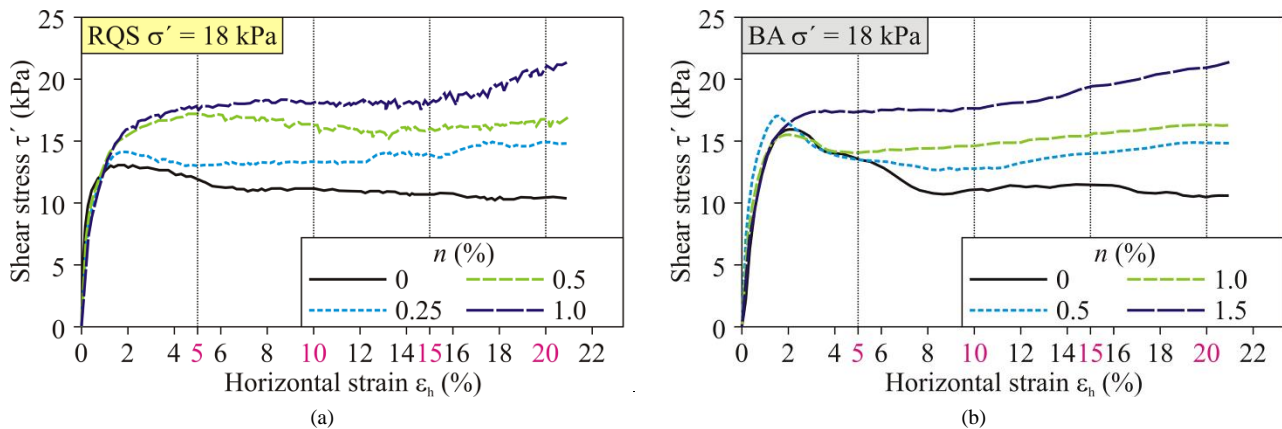


Figure 7. The shear strength curves of (a) RQS and (b) BA for the normal stress of $\sigma' = 18 \text{ kPa}$

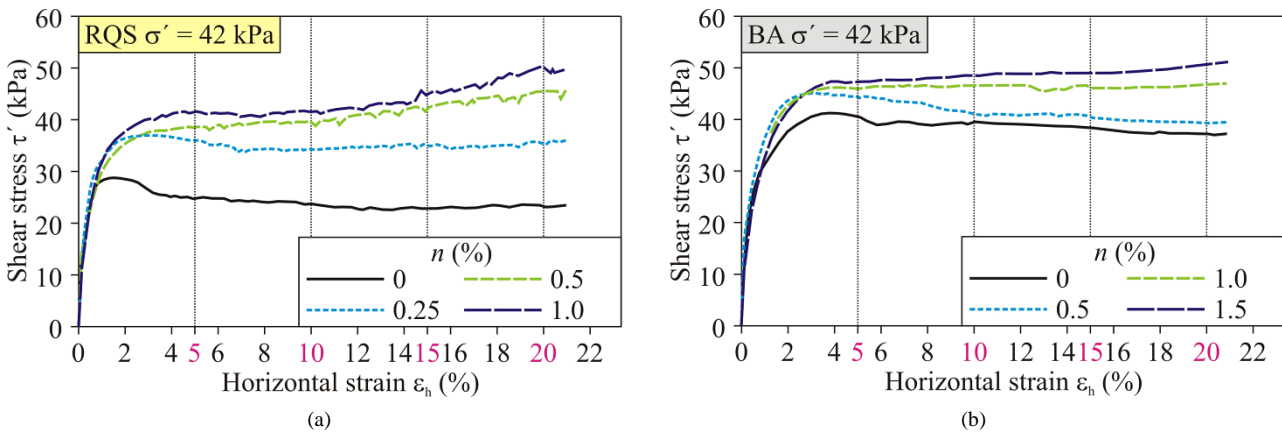


Figure 8. The shear strength curves of (a) RQS and (b) BA for the normal stress of $\sigma' = 42 \text{ kPa}$

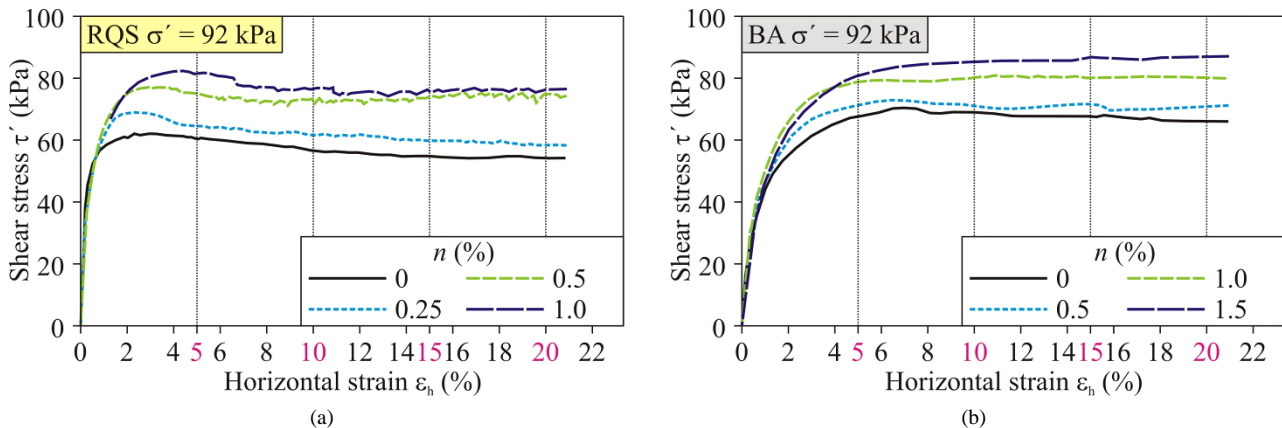


Figure 9. The shear strength curves of (a) RQS and (b) BA for the normal stress of $\sigma' = 92 \text{ kPa}$

The shear strength curves for the parent RQS and BA materials showed a typical shear stress path that could be expected for such material types, i.e., increasing the shear stress τ' up to the peak stress state and subsequently slightly decreasing to the critical stress state, when the shear stress remains constant with an increasing in the horizontal strain ϵ_h [63, 64].

In the case of the materials reinforced with PET rings, the greater peak (the equivalent of the peak) of the shear strength was recorded depending on the degree of reinforcement. After reaching the peak (the equivalent of the peak) shear strength, the course of the shear stress remained constant, e.g., Figures 8-b and 9-b, or even continued to rise slowly with an increase in the horizontal strain, e.g., Figures 7-a and 8-a. Only in some cases was a neglected decrease in the shear strength with an increase in the horizontal strain recorded, e.g., Figures 7-b and 9-b. The stabilization or increase in the shear strength with the increase in the horizontal strain can be attributed to the mobilization of the PET rings in the shear surface area. Since, in many cases, the shear strength increased with an increase in the horizontal strain, the shear strength parameters were determined for the horizontal strain of 5, 10, 15, and 20 %. The Coulomb's failure lines and the shear strength properties, i.e., the effective angle of the shear strength ϕ' and the effective apparent cohesion c' , are given in Figure 10 for $\epsilon_h = 5\%$, Figure 11 for $\epsilon_h = 10\%$, Figure 12 for $\epsilon_h = 15\%$, and Figure 13 for $\epsilon_h = 20\%$.

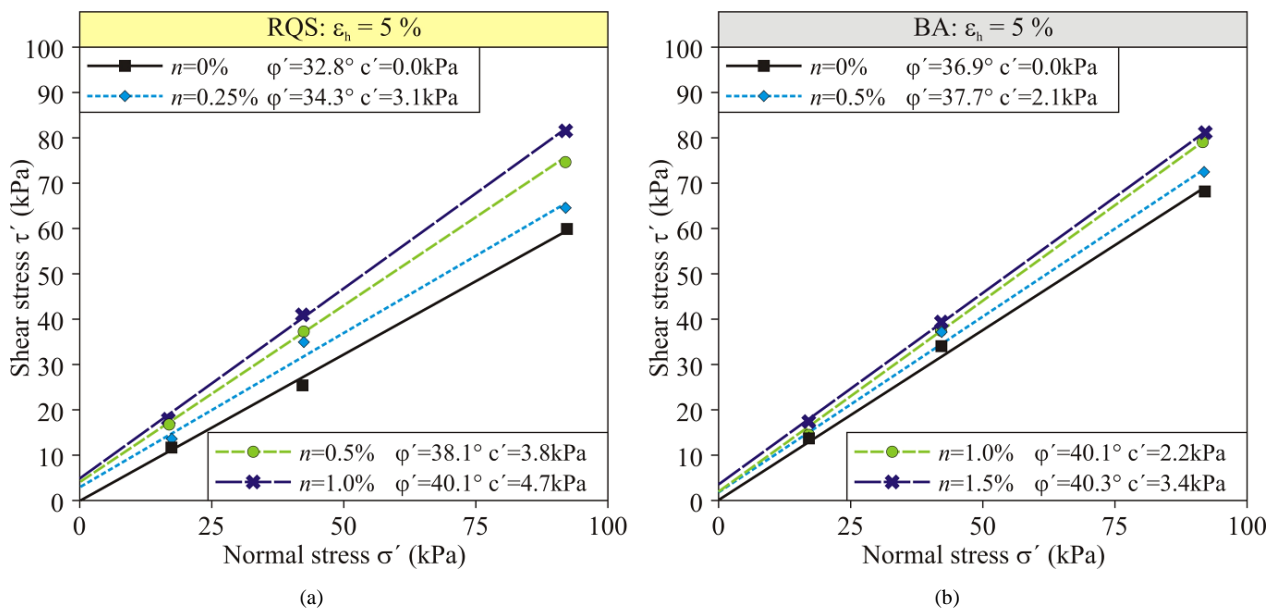


Figure 10. The evaluation of the shear strength tests of (a) RQS and (b) BA for the horizontal strain of $\epsilon_h = 5\%$

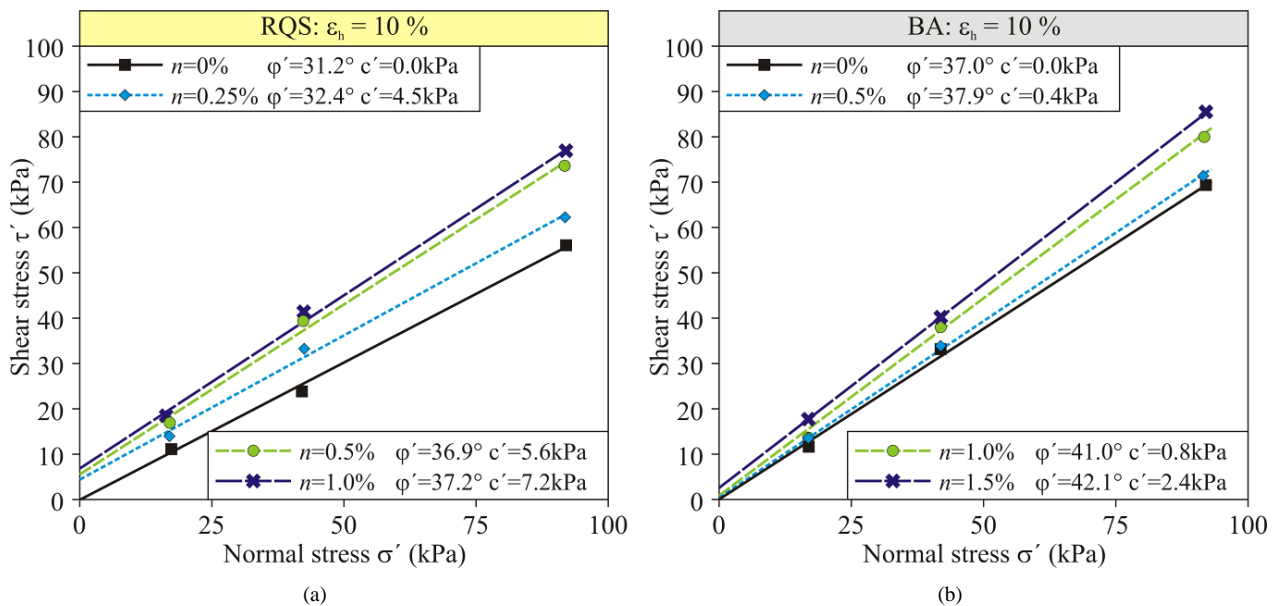


Figure 11. The evaluation of the shear strength tests of (a) RQS and (b) BA for the horizontal strain of $\epsilon_h = 10\%$

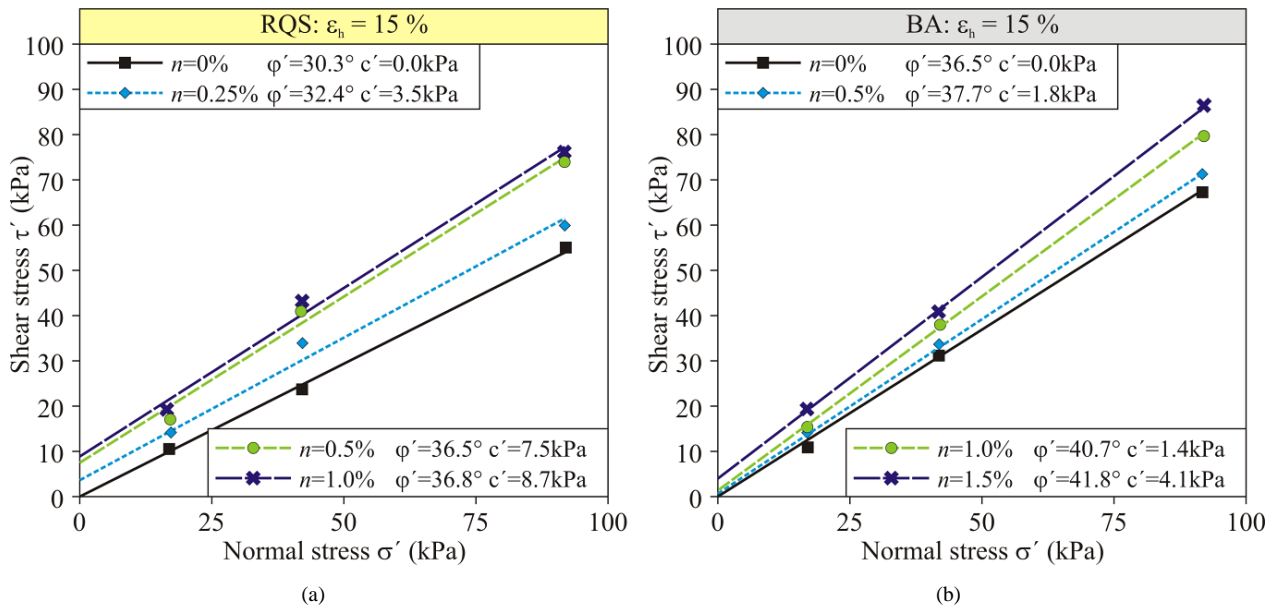


Figure 12. The evaluation of the shear strength tests of (a) RQS and (b) BA for the horizontal strain of $\epsilon_h = 15\%$

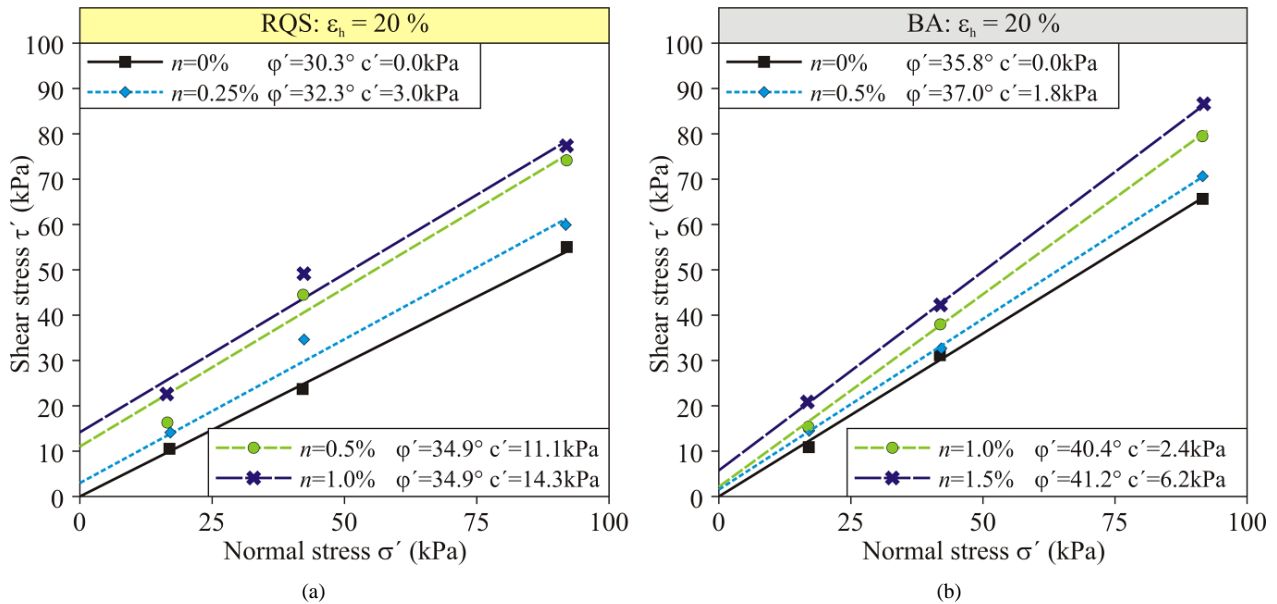


Figure 13. The evaluation of the shear strength tests of (a) RQS and (b) BA for the horizontal strain of $\epsilon_h = 20\%$

The results showed that within the same value of ϵ_h , the angle of the shear strength as well as an increase in the apparent cohesion with increasing the degree of reinforcement n . If the constant value of the degree of reinforcement is considered, for RQS as well as for the BA materials, with an increase in the value of ϵ_h , there is a slight decrease in the angle of the shear strength ϕ' and a slight increase in the apparent cohesion c' . The changes in the shear strength parameters with an increase in ϵ_h are more pronounced in the case of RQS than BA.

The formulas, which exactly define the shear strength of both materials for different degrees of reinforcement and the horizontal strains, are stated in Table 2. Also, the coefficients of determination R^2 are listed. Coulomb's strength line equations are determined with a relatively high degree of accuracy (the lowest R^2 value is 0.948).

The angle of dilatancy for each sample tested, as determined by Equation 4, is presented in Figure 14. The angle of dilatancy was determined individually for each normal stress, i.e., $\sigma' = 18, 42, \text{ and } 92 \text{ kPa}$, as its value decreases with an increase in normal stress [67-69]. For both materials tested, RQS and BA, the reinforcement using PET rings causes an increase in the angle of the dilatancy, regardless of the normal stress value. With the increase in the degree of reinforcement, the value of the dilatancy angle tends to decrease slightly; that is, the highest values of dilatancy angles were determined at the lowest degree of reinforcement, i.e., $n = 0.25\%$ for RQS and $n = 0.50\%$ for BA.

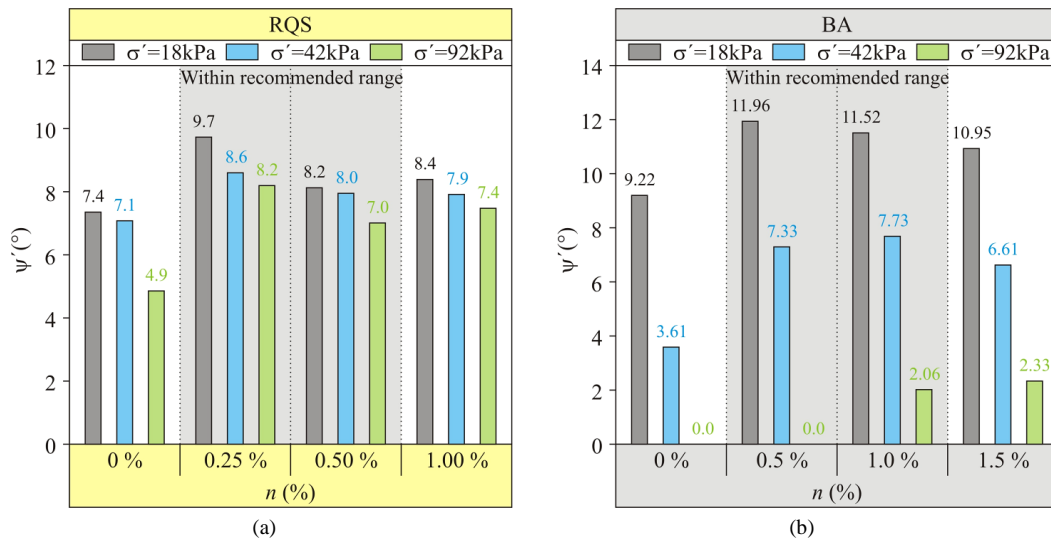


Figure 14. The evaluation of the dilatancy angles: (a) RQS and (b) BA

To evaluate the optimal degree of reinforcement, two dependencies were plotted to demonstrate the impact of the reinforcement:

- The dependence between the τ_r / τ ratio and the degree of reinforcement n , where τ_r represents the shear strength of the sample reinforcement material, and τ represents the shear strength of the sample parent material (Figure 15);
- The dependence between the ϕ_r / ϕ ratio and the degree of reinforcement n , where ϕ_r represents the angle of the shear strength of the sample reinforcement material, and ϕ represents the angle of the shear strength of the sample parent material (Figure 16).

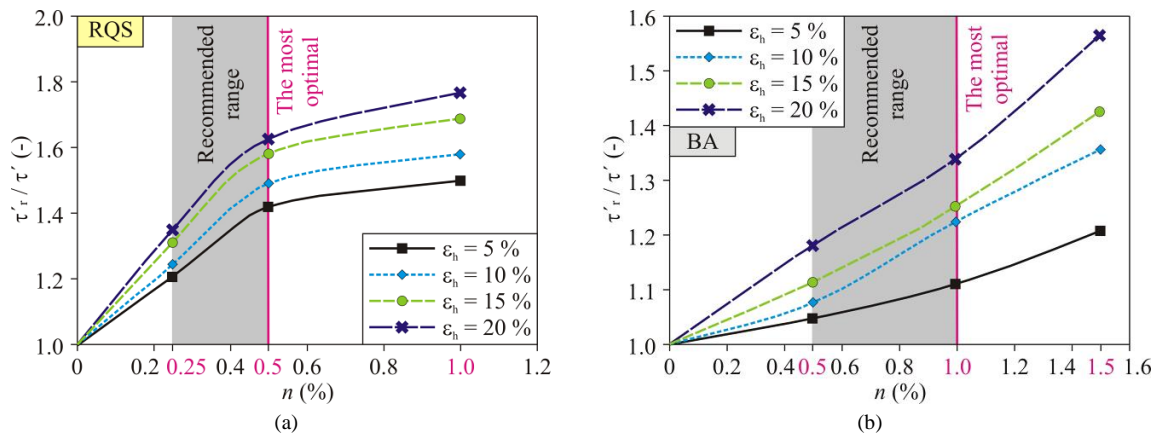


Figure 15. The evaluation of the τ_r / τ ratio for the different values of ϵ_h and reinforcements: (a) RQS and (b) BA

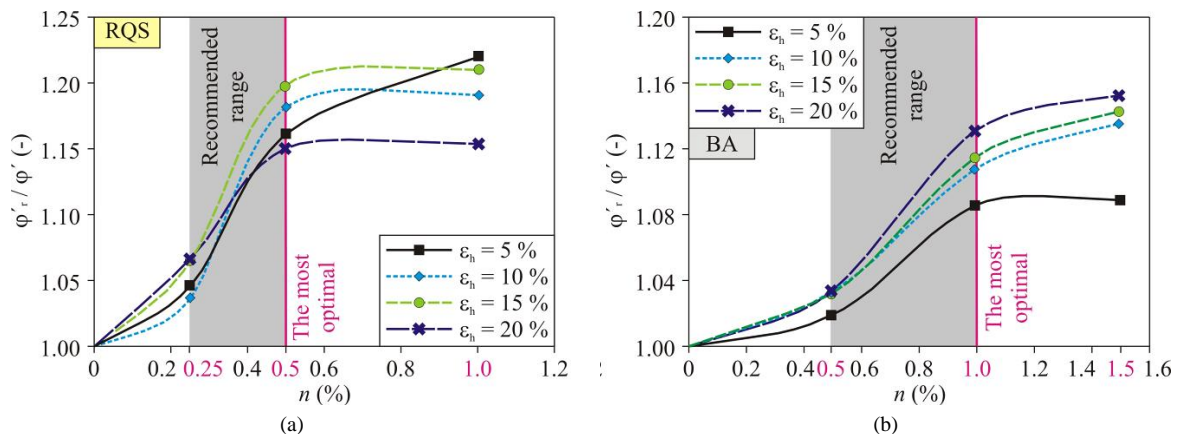


Figure 16. The evaluation of the ϕ_r / ϕ ratio for the different values of ϵ_h and reinforcements: (a) RQS and (b) BA

In the case of RQS (Figures 15-a and 16-a), it can clearly be seen that the ratio of τ_r / τ as well as ϕ_r / ϕ significantly increases up to the degree of reinforcement $n = 0.5\%$. After this value has been overcome, there is only a very slow

increase in the τ_r / τ or ϕ_r / ϕ with an increase in the degree of reinforcement. The optimum degree of reinforcement of RQS is within the range of $n = 0.25 - 0.5 \%$, whilst the most optimum is the value of $n = 0.5 \%$.

In the case of BA (Figures 15-b and 16-b), the ratio of τ_r / τ constantly increases with increases in the degree of reinforcement n (up to $n = 1.5 \%$). The impact of the reinforcement on the apparent cohesion was relatively small. The maximum value, which is only $c' = 6$ kPa, was measured for $\alpha_h = 20 \%$ and $n = 1.5 \%$; this parameter can therefore be ignored. The ϕ_r / ϕ ratio significantly increases only up to $n = 1.0 \%$. Based on these results, it can be stated that BA's optimum degree of reinforcement is within the range of $n = 0.5 - 1.0 \%$, whilst the most optimum is the value of $n = 1.0 \%$. For both materials tested, the τ_r / τ ratio also increases with increases in the α_h , which positively affects the shear strength of the reinforced material and the properties of its shear strength (Table 3).

Table 3. Formulas determined and their accuracy for Coulomb's failure lines

α_h (-)	RQS			BA		
	n (%)	Shear strength		n (%)	Shear strength	
		τ (kPa)	R^2 (-)		τ (kPa)	R^2 (-)
0.05	0	$0.6455\sigma'$	0.993	0	$0.7524\sigma'$	0.995
	0.25	$0.6821\sigma' + 3.07$	0.982	0.50	$0.7717\sigma' + 2.14$	0.994
	0.50	$0.7839\sigma' + 3.80$	0.998	1.00	$0.8422\sigma' + 2.20$	0.997
	1.00	$0.8408\sigma' + 4.68$	0.998	1.50	$0.8470\sigma' + 3.35$	1.000
0.10	0	$0.6059\sigma'$	0.996	0	$0.7551\sigma'$	0.997
	0.25	$0.6334\sigma' + 4.52$	0.989	0.50	$0.7773\sigma' + 0.42$	0.998
	0.50	$0.7503\sigma' + 5.56$	0.990	1.00	$0.8708\sigma' + 0.79$	0.998
	1.00	$0.7595\sigma' + 7.25$	0.995	1.50	$0.9035\sigma' + 2.37$	1.000
0.15	0	$0.5864\sigma'$	0.996	0	$0.7410\sigma'$	0.999
	0.25	$0.6350\sigma' + 3.50$	0.972	0.50	$0.7726\sigma' + 0.80$	1.000
	0.50	$0.7393\sigma' + 7.50$	0.979	1.00	$0.8610\sigma' + 1.41$	0.999
	1.00	$0.7493\sigma' + 8.72$	0.982	1.50	$0.8930\sigma' + 4.07$	1.000
0.20	0	$0.5846\sigma'$	0.999	0	$0.7198\sigma'$	0.998
	0.25	$0.6327\sigma' + 3.03$	0.948	0.50	$0.7523\sigma' + 1.76$	1.000
	0.50	$0.6986\sigma' + 11.1$	0.955	1.00	$0.8522\sigma' + 2.37$	0.999
	1.00	$0.6969\sigma' + 14.271$	0.957	1.50	$0.8761\sigma' + 6.16$	1.000

4.1.2. Deformation Properties of RQS and BA Reinforced by the Distributed PET Rings

The results of the 1D compression modulus E_{1D} are given in Figure 17 for both materials tested. The values of E_{1D} are given for each normal stress, i.e., $\sigma' = 18, 42, \text{ and } 92$ kPa. In the case of RQS (Figure 17-a), the values of E_{1D} are approximately the same as for the sample parent material and the material reinforced by PET rings when $n = 0.25$ and 0.50% . A significant drop in the E_{1D} values of the reinforced RQS was recorded for $n = 1.0 \%$. In the case of BA, the increase in the degree of reinforcement up to $n = 1.0 \%$ led to a slight increase in the E_{1D} values (Figure 17-b), i.e., a 23 % increase in E_{1D} for $\sigma' = 18$ kPa, an 18 % increase in E_{1D} for $\sigma' = 42$ kPa, and a 21 % increase in E_{1D} for $\sigma' = 92$ kPa. However, in the case of BA, a further increase in the degree of reinforcement ($n = 1.5 \%$) led to a significant drop in the E_{1D} values. The ratio of the E_{1D} of the reinforced material (marked $E_{1D,r}$) to the E_{1D} of the parent material (marked E_{1D}) is stated in Figure 18-a for RQS and Figure 18-b for BA.

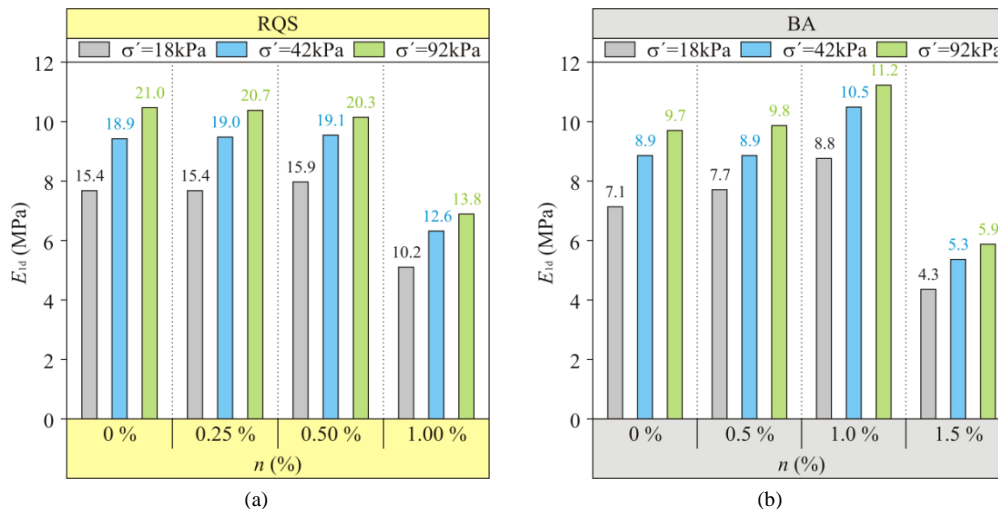


Figure 17. The evaluation of the E_{1D} compression modulus: (a) RQS and (b) BA

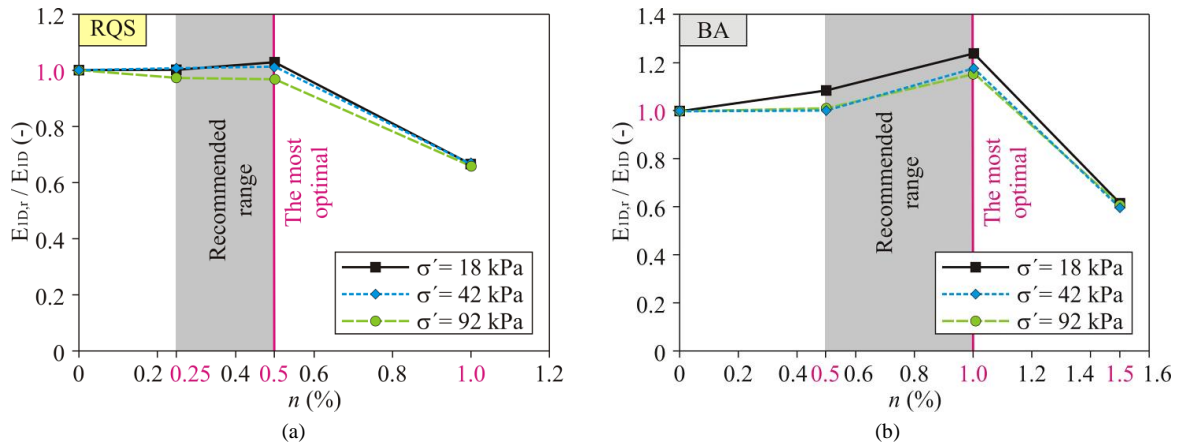


Figure 18. The ratio of the E_{IDr} to E_{ID} for different degree of reinforcement: (a) RQS and (b) BA

When the degree of reinforcement n reaches a relatively high value ($n = 1.0\%$ for RQS or $n = 1.5\%$ for BA), there are too many PET rings in the material tested, leading to the reinforcement material being less compact and having greater compressibility. Based on these results, increasing n by over 0.5% for RQS and 1.0% for BA is not recommended.

4.2. Evaluation of the Physical Modeling

In the case of the physical model, the tests were carried out until a slip area was formed, and the embankment model collapsed. The maximum value of the loading σ that could be applied to the given embankment model during the tests was as follows (increasing the load over these values led to the collapse of the embankment model):

- $\sigma = 87.8$ kPa for the embankment made of the parent RQS;
- $\sigma = 247.0$ kPa for the embankment made of RQS reinforced by the PET rings: $n = 0.25\%$;
- $\sigma = 77.3$ kPa for the embankment made of the parent BA;
- $\sigma = 176.8$ kPa for the embankment made of BA reinforced by the PET rings: $n = 0.5\%$.

The dependence between the ratio h_i / H and $\Delta x / H$ for the loading value $\sigma = 75$ kPa that was achieved in each test is shown in Figure 19, where h_i is the height/position of the horizontal deformation recording (the height of the LVDT sensor from the bottom of the model); Δx is the horizontal deformation measured; and H is the height of the embankment model. The results show that the horizontal deformation mainly occurs in the upper part of the slope when the loading $\sigma = 75$ kPa is applied. The horizontal deformation of the embankment made of the parent BA is almost 2 times greater than for the embankment made of the parent RQS. At this loading stage, the horizontal deformation of the embankments made of the PET ring-reinforced RQS and the PET ring-reinforced BA is almost negligible.

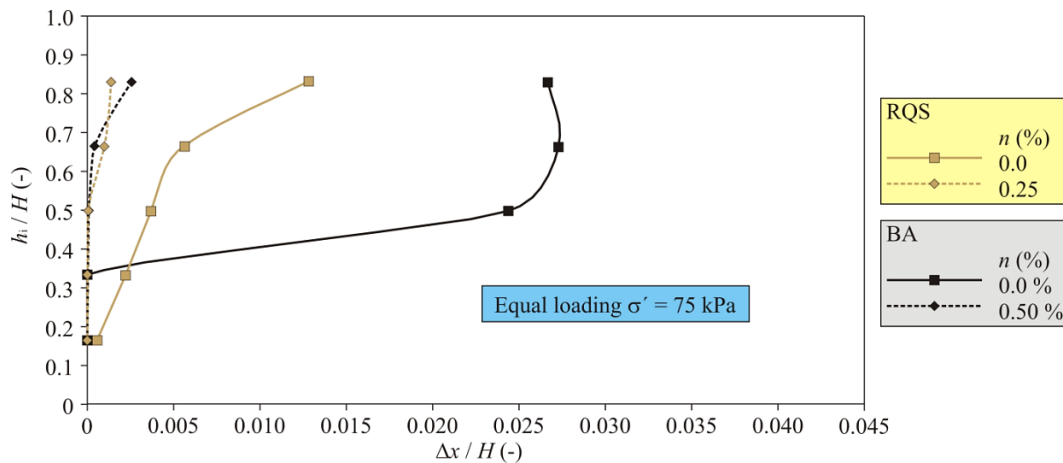


Figure 19. The dependency between h_i / H and $\Delta x / H$ for the equal loading $\sigma' = 75$ kPa

The maximum values of the $\Delta x/H$ ratios reached are presented in Figure 20. Right before the collapse of the model, the maximum values of the $\Delta x/H$ ratio of the embankment made of the parent RQS are similar to those for the embankment made of the PET ring reinforced RQS. However, the loading of the embankment made of the PET ring reinforced RQS was about 2.8 times greater than for the embankment made of the parent RQS. The maximum values of the $\Delta x/H$ ratio of the embankment made of the parent BA were about 75 % of the values measured for the embankment made of BA reinforced by PET rings. However, the embankment made of PET rings reinforced BA resists about a 2.3 times greater loading than the embankment made of the parent BA.

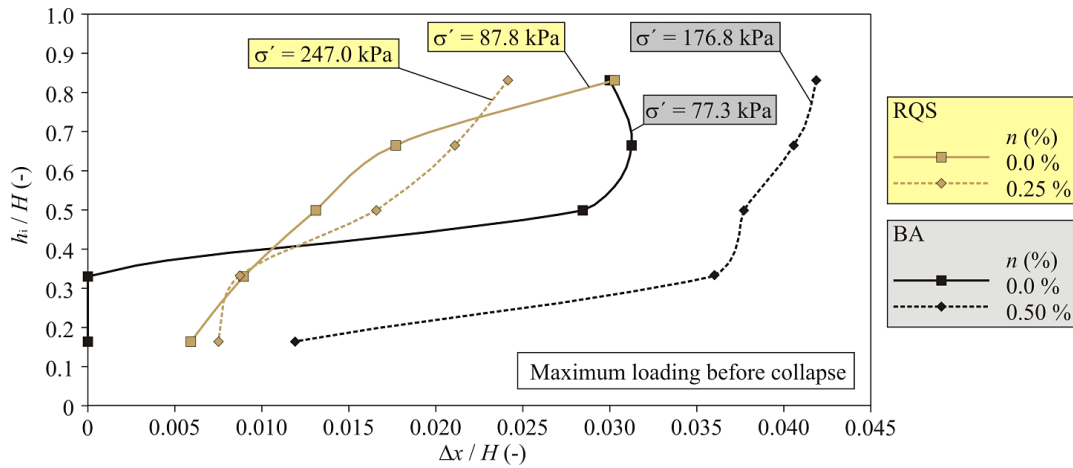


Figure 20. The dependency between h_i / H and $\Delta x / H$ for the maximum loading achieved

The deformations inside the body of the embankment, which were primarily located in the slope section, were monitored using targets, as described in section 4.2. Figure 21-a shows the movement of the targets for the embankment model made of the parent RQS for the loading $\sigma = 87.8$ kPa, and Figure 21-b shows the movement of the targets for the embankment model made of RQS reinforced with PET rings for the loading $\sigma = 247.0$ kPa. The deformations inside the embankment body are similar to each other; no negative aspects were observed in the stress-deformation behavior of the embankment made of the PET ring-reinforced RQS material.

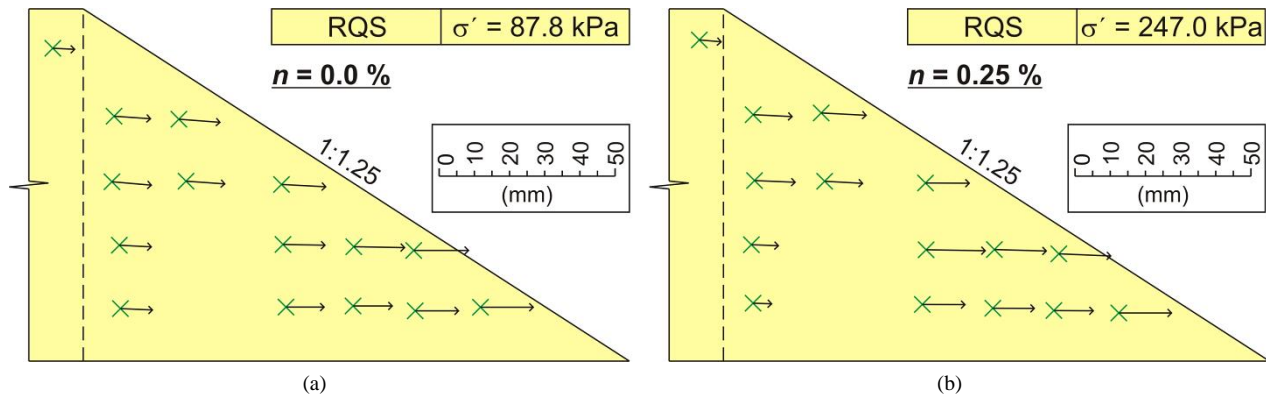


Figure 21. Movement of the targets placed inside the slope: (a) parent RQS and (b) RQS reinforced by PET rings ($n = 0.25\%$)

Figure 22-a shows the movement of the targets for the embankment model made of the parent BA for the loading $\sigma = 77.3$ kPa, and Figure 22-b shows the movement of the targets for the alternative to the embankment made of PET ring reinforced BA for the loading $\sigma = 176.8$ kPa. In comparison to the embankment made of the parent BA, where the deformations are more concentrated in the upper part of the embankment, the deformation of the embankment body and the slope made of BA reinforced by PET rings seems to be more compact (Figure 22-b): the deformation is measured over the entire height of the embankment. Hence, the shear area is close to the bottom of the embankment model. This effect can be attributed to the PET rings that connect the ash grains and, as it were, create a more "compact" material.

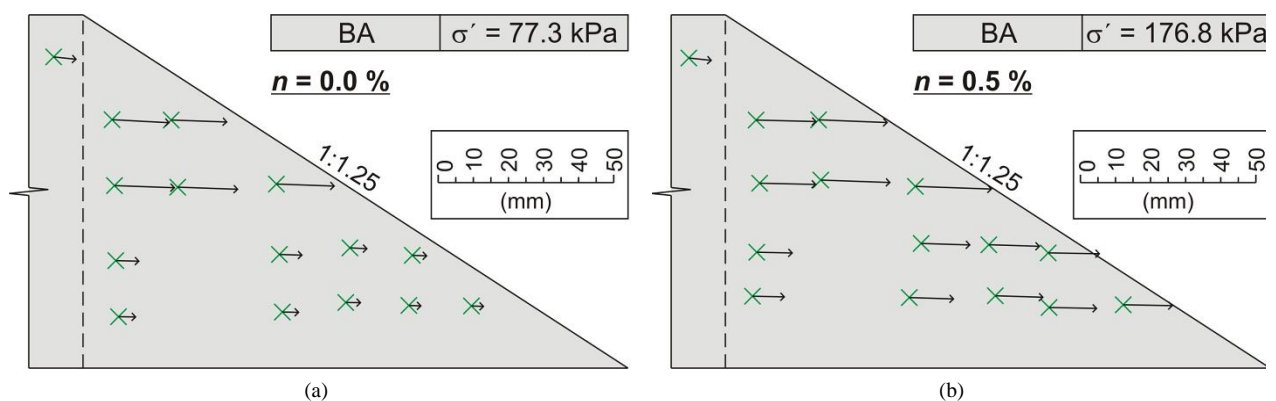


Figure 22. Movement of the targets placed inside the slope: (a) parent BA and (b) BA reinforced by PET rings ($n = 0.50\%$)

The vertical deformations of the embankment models are summarized in Table 4, where Δy_1 and Δy_2 represent the vertical settlement of the front and rear edge of the loading plate (from the side of the slope), and b represents the width of the steel loading plate ($b = 300$ mm). The evaluation was mainly focused on the absolute value of the Δy_1 deformation, $\Delta y_1 / b$ ratio, and uneven settlement $(y_1 - y_2) / b$ for the given loading σ . The results presented clearly show that the distributed PET ring reinforcements have a positive impact on the behavior of the embankment model made of RQS as well as BA.

Table 4. Evaluation of the vertical deformations of the loading plate

Material	σ' (kPa)	Δy_1 (mm)	$\Delta y_1/b$ (%)	$(\Delta y_1 - \Delta y_2)/b$ (%)
RQS	50	5.33	1.78	1.40
	87.8	18.59	6.20	3.71
RQS + PET rings ($n = 0.25$ %)	50	1.33	0.44	0.09
	100	3.84	1.28	0.39
	150	6.69	2.23	0.51
	200	10.97	3.66	0.68
	247	19.35	6.45	1.20
BA	50	10.54	3.51	0.75
	77.3	35.13	11.71	1.85
BA + PET rings ($n = 0.5$ %)	50	4.63	1.54	0.78
	100	11.84	3.95	1.46
	150	21.60	7.20	1.81
	176.8	31.69	10.56	1.90

5. Discussion

The improvement of RQS or BA with distributed PET rings has not yet been analyzed by other authors; however, the values of the degree of reinforcement recommended in this study are similar to those presented by other authors for sand, clay, or fly ash reinforced by different types of fibers [21, 27, 31, 53]. The shear strength properties of RQS can be significantly improved by adding PET rings in the degree of reinforcement range of $n = 0.25 - 0.50$ %, while the highest increase in the shear strength can be expected when $n = 0.50$ %. In the case of the BA, which is based on the ϕ'_v/ϕ' ratio, the optimal range of the degree of reinforcement $n = 0.50 - 1.0$ % can be recommended, while the highest increase in the shear strength can be achieved when $n = 1.00$ %. These results correspond to those published by, e.g., [25, 31, 41], for the sandy soils reinforced using PET fibers. They stated that the optimum degree of reinforcement n is up to $0.75 - 1.00$ %. The optimum degree of reinforcement $n = 1.00$ % was declared also by Zhu et al. [47]. They analyzed clayey soils reinforced using PET strips. The degrees of reinforcement recommended for RQS and BA materials in the present study can be similar to those used to reinforce fine-grained and sandy materials using PET fibers or strips. Existing studies have shown that the shear strength of a reinforced material can increase slightly even after exceeding the optimal degree of reinforcement; for example, the summary of results presented by Khalid & Alshawmar [41]. In the study presented, the shear strength of the reinforced RQS and BA continued to increase with increases in the degree of reinforcement above the recommended ones; this was more significant for BA and less critical for RQS. While the angle of shear strength only slightly increased, the increase in apparent cohesion was more pronounced. In the case of a higher degree of reinforcement, i.e., $n = 1.0$ % or RQS and $n = 1.5$ % for BA, there was a significant decrease in the compressibility modulus (described below), leading to the conclusion that a higher degree of reinforcement does not produce the desired improvement effect. An increase in the dilatancy angles was also observed for the RQS and BA reinforced by the distributed PET rings, similar to the results presented by Sadek et al. [33]. Inhibition of the dilatancy, which was observed by Michalowski & Čermák [70] and Gray & Ohashi [71], has not been recorded for the reinforced materials tested.

The compression tests showed that the 1D compression modulus of the deformation of the materials reinforced by the PET rings remained similar (RQS) or slightly increased (BA) in comparison to the parent materials; however, after exceeding the optimal degree of reinforcement ($n \leq 0.5\%$ for RQS and $n \leq 1.0\%$ for BA), a significant decrease in the 1D compression modulus occurred. This effect has been mainly attributed to the problem with preparing the reinforced samples. Too many PET rings caused the vertical compaction to be insufficiently effective and led to "small cavities" between the PET rings apparently being formed, which ultimately led to the higher compressibility of the reinforced samples. Similar results were observed by Zhu et al. [47] for expansive clay reinforced by PET strips. They stated that the stiffness of the reinforced sample decreased when the degree of reinforcement exceeded about $n = 1\%$. They attributed this finding to the large voids within the material matrix, which were formed at a high degree of reinforcement. Since a high degree of reinforcement was not optimal even in terms of shear strength, it was not justified to search for a way to eliminate the decrease in the compressibility of the reinforced samples (for example, by vibrating).

Reinforcement of FA using PET rings has been investigated by Lal & Mandal [58] and Nadaf & Mandal [59]. However, in all these studies, the PET rings were connected to each other and created a "cellular reinforcement." Their studies have shown that this type of reinforcement can also offer significant benefits when building a geotechnical structure; however, manually connecting PET rings can be considered very laborious and time-consuming. In the presented study, PET rings were used as randomly distributed reinforcement. Mixing PET rings with the parent material is a simple process. The only thing to be careful about is thoroughly mixing the PET rings with the parent material to avoid clumping. The use of PET rings as randomly distributed reinforcement has not been investigated before, which makes the presented study unique.

Physical modeling allows for a detailed investigation of the behavior of a reinforced earth body, as demonstrated by previous studies [56-59]. Since the authors applied a different type of reinforcement and parent material in these studies, a mutual comparison of their results with the results presented in this study was considered unfounded. However, the physical model of the embankment presented in this study clearly demonstrated that the distributed PET ring reinforcements positively strengthen the embankment body and significantly reduce its deformation behavior. The results showed that the embankment model made of RQS reinforced with the distributed PET rings can resist up to 2.8 times greater loading than its alternative made of the parent RQS. In contrast, the deformation of the embankment slope remains approximately the same. The embankment model made of BA reinforced with the distributed PET rings resisted up to 2.3 times greater loading than the model made of the parent BA, while the horizontal deformation of the slope increased only by about 1.3 times. The physical model was executed only for the lowest degrees of reinforcement of the RQS and BA materials, i.e., $n = 0.25\%$ for RQS and $n = 0.50\%$ for BA. The physical models were not performed for higher degrees of reinforcement, as the PET ring cutting process is currently not automated and tests with higher degrees of reinforcement require manual cutting of a large amount of PET ring. Due to the size of the physical model, this was evaluated as unjustifiable at the current study stage since even the lower degrees of reinforcement proved their validity.

We plan to build a smaller embankment in the future for the cycle path made of tested reinforced materials, which permits supplementing the present study with the results of monitoring an actual construction.

6. Conclusion

This paper presents the results of testing coarse-grained waste materials, such as rock quarry sand (RQS) and bottom ash (BA), which were improved using randomly distributed reinforcements made of polyethylene terephthalate (PET) rings. The PET rings used as reinforcements were created by cutting non-recycled 0.5 liter PET bottles with a diameter of about 50 - 60 mm and a thickness of about 10 mm. The shear strength properties of the RQS and BA reinforced by the randomly distributed PET rings were tested using large-sized direct shear tests. The compression tests allowed for determining the 1D deformation modulus, which were evaluated based on the same principles used for oedometer compression tests. The results of the laboratory testing can be summarized by the following points:

- The shear strength properties of the reinforced materials remain constant or slightly increase with an increase in the horizontal strain after reaching the peak shear strength. A negligible decrease was recorded only in the case of RQS when $\sigma' = 92$ kPa or BA when $\sigma' = 18$ kPa and $n = 0.5 - 1.0\%$. As a result, the shear strength properties were evaluated at $\varepsilon_h = 5, 10, 15,$ and 20% .
- The optimum degree of reinforcement n of RQS is within the range of $n = 0.25 - 0.5\%$, whilst the most optimum was the value of $n = 0.5\%$. For this degree of reinforcement, the shear strength of the reinforced RQS was improved by about 1.42 times for $\varepsilon_h = 5\%$ up to about 1.63 times for $\varepsilon_h = 20\%$. The angle of the shear strength of the reinforced RQS was improved by about 1.16 times for $\varepsilon_h = 5\%$ and about 1.15 times for $\varepsilon_h = 20\%$. The apparent cohesion of the reinforced RQS increased from about 3.8 kPa to about 11.1 kPa (when $n = 0.5\%$). Increasing the n value above 0.5% was associated with a significant drop in the 1D compression modulus of the deformation.
- In the case of BA, the optimum degree of reinforcement n was within the range of $n = 0.5 - 1.0\%$, whilst the most optimum seems to be $n = 1.0\%$. The shear strength of the reinforced BA with the optimum degree of reinforcement was improved by about 1.11 times for $\varepsilon_h = 5\%$ up to about 1.34 times for $\varepsilon_h = 20\%$. The increase in the shear strength was also determined for the reinforced BA when $n = 1.5\%$; however, at this degree of reinforcement, a significant drop in the 1D compression modulus of the deformation was observed.
- Reinforcing RQS as well as BA with PET rings led to an increase in the dilatancy angle for all the degrees of reinforcement tested.

The results of the physical modeling confirmed the positive effect of the distributed PET ring reinforcement on the mechanical behavior of the RQS and BA materials. The embankment model made of RQS reinforced by the distributed PET rings resisted 2.8 times greater loading in a similar deformation than the embankment model made of the parent RQS. The embankment model made of BA reinforced by the distributed PET rings, even for the degree of reinforcement $n = 0.5\%$, resisted up to 2.3 times greater loading than the embankment model made of parent BA, while the deformation increased only about 1.3 times.

The presented study thus clearly demonstrated that when building geotechnical structures, traditional materials such as gravel and quarry aggregates can be effectively replaced by alternative materials like RQS and BA. These materials' strength and deformation parameters can also be significantly improved using randomly distributed reinforcement in the form of PET rings, a previously unexplored reinforcement type. The presented study also showed that PET rings, used as randomly distributed reinforcement, can be an equally effective reinforcing material such as fibers, strips, and flakes.

7. Declarations

7.1. Author Contributions

Conceptualization, M.S.; methodology, J.S., I.S., M.S., and M.K.; investigation, J.S., I.S., M.S., and M.K.; writing—original draft preparation, J.S.; writing—review and editing, J.S., I.S., and M.S.; visualization, J.S.; supervision, I.S. All authors have read and agreed to the published version of the manuscript.

7.2. Data Availability Statement

The data presented in this study are available on request from the corresponding author.

7.3. Funding

The authors received no financial support for the research, authorship, and/or publication of this article.

7.4. Acknowledgements

The creating and equipment of the physical model presented in this study was supported by the Techkon, s.r.o., company with no financial interests.

7.5. Conflicts of Interest

The authors declare no conflict of interest.

8. References

- [1] Allen, T. M., & Bathurst, R. J. (2014). Design and Performance of 6.3-m-High, Block-Faced Geogrid Wall Designed Using K-Stiffness Method. *Journal of Geotechnical and Geoenvironmental Engineering*, 140(2), 12. doi:10.1061/(asce)gt.1943-5606.0001013.
- [2] Drusa, M., Vlček, J., Holičková, M., & Kais, L. (2016). Analytical and Numerical Evaluation of Limit States of MSE Wall Structure. *Civil and Environmental Engineering*, 12(2), 145–152. doi:10.1515/cee-2016-0020.
- [3] Scotland, I., Dixon, N., Frost, M., Fowmes, G., & Horgan, G. (2016). Modelling deformation during the construction of wrapped Geogrid-reinforced structures. *Geosynthetics International*, 23(3), 219–232. doi:10.1680/jgein.15.00049.
- [4] Sulovska, M., & Stacho, J. (2021). Analysis of Geogrid Reinforced Structures with a Passive Facing System Using Different Computational Methods. *Civil and Environmental Engineering*, 17(2), 500–512. doi:10.2478/cee-2021-0052.
- [5] Sulovska, M. (2019). Design Of A Road Embankment Reinforced Using A Geogrid. 19th International Multidisciplinary Scientific GeoConference SGEM2019, Ecology, Economics, Education and Legislation. doi:10.5593/sgem2019/1.2/s02.019.
- [6] Arulrajah, A., Abdullah, A., Bo, M. W., & Bouazza, A. (2009). Ground improvement techniques for railway embankments. *Proceedings of the Institution of Civil Engineers: Ground Improvement*, 162(1), 3–14. doi:10.1680/grim.2009.162.1.3.
- [7] Esen, A. F., Woodward, P. K., Laghrouche, O., Čebašek, T. M., Brennan, A. J., Robinson, S., & Connolly, D. P. (2021). Full-scale laboratory testing of a geosynthetically reinforced soil railway structure. *Transportation Geotechnics*, 28(1), 12. doi:10.1016/j.trgeo.2021.100526.
- [8] Yonezawa, T., Yamazaki, T., Tateyama, M., & Tatsuoka, F. (2014). Design and construction of geosynthetic-reinforced soil structures for Hokkaido high-speed train line. *Transportation Geotechnics*, 1(1), 3–20. doi:10.1016/j.trgeo.2013.12.001.
- [9] Blackwood, T. W., & Vulova, C. V. (2006). Geogrid Reinforced Embankment Constructed over Peat Soils in Clark County, Washington: Design and Field Performance. *Airfield and Highway Pavement*, 317–328. doi:10.1061/40838(191)27.
- [10] Hu, Y., Li, H., Wang, X., Wang, Q. A., & Zhang, X. (2011). Application of Geogrid in Widening Highway Embankment. *ICCTP 2011*, 3059–3066. doi:10.1061/41186(421)304.
- [11] Liu, K. F., Feng, W. Q., Cai, Y. H., Xu, H., & Wu, P. C. (2023). Physical model study of pile type effect on long-term settlement of geosynthetic-reinforced pile-supported embankment under traffic loading. *Transportation Geotechnics*, 38(1), 12. doi:10.1016/j.trgeo.2022.100923.
- [12] Zheng, G., Xia, B., Zhou, H., Yu, X., & Diao, Y. (2023). Influence of deep-cement-mixing column rows on the performance of geosynthetics-reinforced column-supported railway embankment. *Transportation Geotechnics*, 41(1), 14. doi:10.1016/j.trgeo.2023.101012.

- [13] Vega-Meyer, R., & Shao, Y. (2005). Geogrid-Reinforced and Pile-Supported Roadway Embankment. *Contemporary Issues in Foundation Engineering*, 1–13. doi:10.1061/40777(156)9.
- [14] Rahmawati, C., Aisyah, S., Maulana, M. M., & Ahmad, J. (2024). Artificial Intelligence Models for Predicting the Compressive Strength of Geopolymer Cements. *Civil Engineering Journal*, 10, 37-50. doi:10.28991/CEJ-SP2024-010-03.
- [15] Kumar, P., & Singh, S. P. (2008). Fiber-reinforced fly ash subbases in rural roads. *Journal of Transportation Engineering*, 134(4), 171–180. doi:10.1061/(ASCE)0733-947X(2008)134:4(171).
- [16] Bacco, C. E. R., Parga-Montoya, N., Landeros, M. D. C. M., Cortés-Palacios, H. A., & Vidales, M. Y. G. (2024). Analysis of the Establishment, Development and Future of Agricultural Reconversion. *Journal of Human, Earth, and Future*, 5(4), 543-559. doi:10.28991/HEF-2024-05-04-01.
- [17] Heineck, K. S., Coop, M. R., & Consoli, N. C. (2005). Effect of Microreinforcement of Soils from Very Small to Large Shear Strains. *Journal of Geotechnical and Geoenvironmental Engineering*, 131(8), 1024–1033. doi:10.1061/(asce)1090-0241(2005)131:8(1024).
- [18] Wu, D., Wang, C., Liu, H., Liu, X., Wang, H., & Wang, Q. (2024). Recycled polyester fiber reinforcing red mud-improved volcanic ash as a sustainable construction material. *Construction and Building Materials*, 413(1), 11. doi:10.1016/j.conbuildmat.2023.134821.
- [19] Paul, J. V., & Sneha, A. R. M. (2016). Effect of random inclusion of bamboo fibers on strength behaviour of flyash treated black cotton soil. *International Journal of Civil Engineering and Technology*, 7(5), 153–160.
- [20] Dandin, S., & Kulkarni, M. (2022). Effect of isolated footing on fly ash subgrade reinforced with PET bottles: An experimental and analytical study. *Construction and Building Materials*, 353(1), 14. doi:10.1016/j.conbuildmat.2022.129095.
- [21] Valipour, M., Shourijeh, P. T., & Mohammadinia, A. (2021). Application of recycled tire polymer fibers and glass fibers for clay reinforcement. *Transportation Geotechnics*, 27(1), 14. doi:10.1016/j.trgeo.2020.100474.
- [22] EsmailpourShirvani, N., TaghaviGhalesari, A., Khaleghnejad Tabari, M., & Janalizadeh Choobbasti, A. (2019). Improvement of the engineering behavior of sand-clay mixtures using kenaf fiber reinforcement. *Transportation Geotechnics*, 19, 1–8. doi:10.1016/j.trgeo.2019.01.004.
- [23] Nugroho, S. A., Wardani, S. R., Muntohar, A. S., & Satibi, S. (2024). Effect of Coal Combustion Waste on Cement-Treated Clay. *Civil Engineering Journal*, 10(11), 3603-3612. doi:10.28991/CEJ-2024-010-11-010.
- [24] Kumar, A., Walia, B. S., & Bajaj, A. (2007). Influence of Fly Ash, Lime, and Polyester Fibers on Compaction and Strength Properties of Expansive Soil. *Journal of Materials in Civil Engineering*, 19(3), 242–248. doi:10.1061/(asce)0899-1561(2007)19:3(242).
- [25] Dang, L. C., & Khabbaz, H. (2019). Shear Strength Behaviour of Bagasse Fibre Reinforced Expansive Soil. *IACGE 2018*, 393–402. doi:10.1061/9780784482049.038.
- [26] Tiwari, N., Satyam, N., & Puppala, A. J. (2021). Strength and durability assessment of expansive soil stabilized with recycled ash and natural fibers. *Transportation Geotechnics*, 29(1), 9. doi:10.1016/j.trgeo.2021.100556.
- [27] Balani, D. M. P., Kikumoto, M., & Cui, Y. (2023). Enhanced sand strength through low-density polyethylene reinforcement. *Construction and Building Materials*, 409(1), 10. doi:10.1016/j.conbuildmat.2023.133928.
- [28] Festugato, L., Flórez Gálvez, J. H., Dias Miguel, G., & Consoli, N. C. (2022). Cyclic response of fibre reinforced dense sand. *Transportation Geotechnics*, 37(1). doi:10.1016/j.trgeo.2022.100811.
- [29] Ghadr, S. (2020). Effect of grain size on undrained anisotropic behaviour of sand–fibre composite. *Transportation Geotechnics*, 22(1), 15. doi:10.1016/j.trgeo.2020.100323.
- [30] Namjoo, A. M., Jafari, K., & Toufigh, V. (2020). Effect of particle size of sand and surface properties of reinforcement on sand-geosynthetics and sand–carbon fiber polymer interface shear behavior. *Transportation Geotechnics*, 24(1), 18. doi:10.1016/j.trgeo.2020.100403.
- [31] Hasanzadeh, A., & Shooshpasha, I. (2023). PET fiber reinforcement efficiency in the mechanical and microstructural characteristics of cemented sand modified with silica fume. *Construction and Building Materials*, 397(1), 17. doi:10.1016/j.conbuildmat.2023.132363.
- [32] Ferreira, J. W. dos S., Senez, P. C., & Casagrande, M. D. T. (2021). Pet fiber reinforced sand performance under triaxial and plate load tests. *Case Studies in Construction Materials*, 15(1), 13. doi:10.1016/j.cscm.2021.e00741.
- [33] Sadek, S., Najjar, S. S., & Freiha, F. (2010). Shear Strength of Fiber-Reinforced Sands. *Journal of Geotechnical and Geoenvironmental Engineering*, 136(3), 490–499. doi:10.1061/(asce)gt.1943-5606.0000235.

- [34] Narani, S. S., Abbaspour, M., Mir Mohammad Hosseini, S. M., & Moghadas Nejad, F. (2020). Long-term dynamic behavior of a sandy subgrade reinforced by Waste Tire Textile Fibers (WTTFs). *Transportation Geotechnics*, 24(1), 11. doi:10.1016/j.trgeo.2020.100375.
- [35] Tang, C.-S., Wang, D.-Y., Cui, Y.-J., Shi, B., & Li, J. (2016). Tensile Strength of Fiber-Reinforced Soil. *Journal of Materials in Civil Engineering*, 28(7), 13. doi:10.1061/(asce)mt.1943-5533.0001546.
- [36] Li, C., & Zornberg, J. G. (2019). Shear Strength Behavior of Soils Reinforced with Weak Fibers. *Journal of Geotechnical and Geoenvironmental Engineering*, 145(9), 7. doi:10.1061/(asce)gt.1943-5606.0002109.
- [37] Tran, K. Q., Satomi, T., & Takahashi, H. (2018). Effect of waste cornsilk fiber reinforcement on mechanical properties of soft soils. *Transportation Geotechnics*, 16, 76–84. doi:10.1016/j.trgeo.2018.07.003.
- [38] Estabragh, A. R., Bordbar, A. T., & Javadi, A. A. (2011). Mechanical Behavior of a Clay Soil Reinforced with Nylon Fibers. *Geotechnical and Geological Engineering*, 29(5), 899–908. doi:10.1007/s10706-011-9427-8.
- [39] Kumar, S., Sahu, A. K., & Naval, S. (2021). Study on the swelling behavior of clayey soil blended with geocell and jute fibre. *Civil Engineering Journal (Iran)*, 7(8), 1327–1340. doi:10.28991/cej-2021-03091728.
- [40] Sharma, Y., Purohit, D. G. M., & Sharma, S. (2017). Improvement of soil properties by using jute fibre as soil stabilizer. *American Journal of Engineering Research*, 6(10), 123-129.
- [41] Khalid, B., & Alshawmar, F. (2024). Comprehensive Review of Geotechnical Engineering Properties of Recycled Polyethylene Terephthalate Fibers and Strips for Soil Stabilization. *Polymers*, 16(13), 31. doi:10.3390/polym16131764.
- [42] Hedayati-Dezfooli, M., Mehdi Moayyedean, Ali Dinc, Mostafa Abdrabbob, Ahmed Saber, and A. M. Amer. "Optimizing Injection Molding for Propellers with Soft Computing, Fuzzy Evaluation, and Taguchi Method." *Emerging Science Journal* 8, no. 5 (2024): 2101-2119. doi:10.28991/ESJ-2024-08-05-025.
- [43] Cai, Y., Shi, B., Ng, C. W. W., & Tang, C. (2006). Effect of polypropylene fibre and lime admixture on engineering properties of clayey soil. *Engineering Geology*, 87(3–4), 230–240. doi:10.1016/j.enggeo.2006.07.007.
- [44] Sukontasukkul, P., & Jamsawang, P. (2012). Use of steel and polypropylene fibers to improve flexural performance of deep soil-cement column. *Construction and Building Materials*, 29, 201–205. doi:10.1016/j.conbuildmat.2011.10.040.
- [45] Shah, A., & Thaker, T. (2025). Enhancing Soil Subgrade Strength Using Waste Plastic Water Bottles as a Reinforcement. *Geo-EnvironMeet 2025*, 283–290. doi:10.1061/9780784485705.030.
- [46] Islam, M. R., Khan, Md. Z. A., Islam, Md. R., Islam, N., Azam, M. S., Ahmed, T., & Roy, K. (2025). A Sustainable Soil Stabilization Technique Using Medical Waste Incineration Ash, Coal-Based Fly Ash, and Polyethylene Terephthalate Strips. *Journal of Materials in Civil Engineering*, 37(4). doi:10.1061/jmcee7.mteng-18665.
- [47] Zhu, J., Saberian, M., Li, J., Maqsood, T., & Yang, W. (2023). Performance of clay soil reinforced with PET plastic waste subjected to freeze-thaw cycles for pavement subgrade application. *Cold Regions Science and Technology*, 214(1), 15. doi:10.1016/j.coldregions.2023.103957.
- [48] Louzada, N. dos S. L., Malko, J. A. C., & Casagrande, M. D. T. (2019). Behavior of Clayey Soil Reinforced with Polyethylene Terephthalate. *Journal of Materials in Civil Engineering*, 31(10). doi:10.1061/(asce)mt.1943-5533.0002863.
- [49] Sivakumar Babu, G. L., & Raja Jaladurgam, M. E. (2014). Strength and Deformation Characteristics of Fly Ash Mixed with Randomly Distributed Plastic Waste. *Journal of Materials in Civil Engineering*, 26(12), 7. doi:10.1061/(asce)mt.1943-5533.0001014.
- [50] Fareghian, M., Afrazi, M., & Fakhimi, A. (2023). Soil Reinforcement by Waste Tire Textile Fibers: Small-Scale Experimental Tests. *Journal of Materials in Civil Engineering*, 35(2), 14. doi:10.1061/(asce)mt.1943-5533.0004574.
- [51] Dandin, S., Sathe, S., Wagale, M., & Jomde, A. (2024). Utilizing PET bottles for sustainable cellular reinforcement: A study on enhancing fly ash backfill bearing strength with innovative geocell alternative. *Construction and Building Materials*, 433(1), 11. doi:10.1016/j.conbuildmat.2024.136641.
- [52] Zhao, Y., Yang, Y., Ling, X., Gong, W., Li, G., & Su, L. (2021). Dynamic behavior of natural sand soils and fiber reinforced soils in heavy-haul railway embankment under multistage cyclic loading. *Transportation Geotechnics*, 28(1), 11. doi:10.1016/j.trgeo.2020.100507.
- [53] Hazirbaba, K. (2017). Large-scale direct shear and CBR performance of geofibre-reinforced sand. *Road Materials and Pavement Design*, 19(6), 1350–1371. doi:10.1080/14680629.2017.1310667.
- [54] Nguyen, G. (2019). Laboratory Study of Soil Shear Strength Improvement with Polyester Fibres. *Fibres & Textiles in Eastern Europe*, 27(2(134)), 90–99. doi:10.5604/01.3001.0012.9993.

- [55] Aouf, G., Alhakim, G., & Jaber, L. (2024). Utilizing Recycled Rubber and Municipal Waste Incineration Fly Ash in Cement-Stabilized Clayey Soils. *Civil Engineering Journal*, 10(11), 3721-3737.
- [56] Khan, B. J., Ahmad, M., Sabri, M. M. S., Ahmad, I., Zamin, B., & Niekurzak, M. (2022). Experimental and Numerical Evaluation of Mechanically Stabilized Earth Wall with Deformed Steel Bars Embedded in Tire Shred-Sand Mixture. *Buildings*, 12(5), 17. doi:10.3390/buildings12050548.
- [57] Vlček, J., Drusa, M., Gago, F., & Mihálik, J. (2023). Analysis of a Large-Scale Physical Model of Geosynthetic-Reinforced Piled Embankment and Analytical Design Methods. *Buildings*, 13(6), 21. doi:10.3390/buildings13061464.
- [58] Lal, B. R. R., & Mandal, J. N. (2013). Effect of Reinforcement Coverage Ratio on Cellular Reinforced Fly Ash Walls. *Geo-Congress*, 72–81. doi:10.1061/9780784412787.008.
- [59] Nadaf, M. B., & Mandal, J. N. (2017). Behavior of Reinforced Fly Ash Slopes with Cellular Mattress and Strips under Strip Loading. *Journal of Hazardous, Toxic, and Radioactive Waste*, 21(4), 13. doi:10.1061/(asce)hz.2153-5515.0000376.
- [60] ICIS. (2022). Independent Commodity Intelligence Service: PET Market in Europe. State of Play. Production, Collection & Recycling. ICISL, London, United Kingdom. Available online: <https://www.icis.com/explore/resources/pet-market-state-of-play-2022/> (accessed on April 2025).
- [61] Dandin, S., Sathe, S., Wagale, M., & Jomde, A. (2024). Utilizing PET bottles for sustainable cellular reinforcement: A study on enhancing fly ash backfill bearing strength with innovative geocell alternative. *Construction and Building Materials*, 433, 136641. doi:10.1016/j.conbuildmat.2024.136641.
- [62] Choudhary, A. K., Jha, J. N., & Fulambarkar, S. (2019). Strength and Deformation Characteristics of Bottom-Ash Reinforced with Single Geocell Mattress Made of Waste Pet Bottles. *Geo-Congress 2019*, 263–272. doi:10.1061/9780784482148.027.
- [63] Stacho, J., & Sulovska, M. (2022). Shear Strength Properties of Coarse-Grained Soils Determined Using Large-Size Direct Shear Test. *Civil and Environmental Engineering*, 18(1), 244–257. doi:10.2478/cee-2022-0023.
- [64] Atkinson, J. (2017). *The mechanics of soils and foundations*. CRC press, Boca Raton, United States. doi:10.1201/9781315273549.
- [65] Simoni, A., & Houlsby, G. T. (2006). The direct shear strength and dilatancy of sand-gravel mixtures. *Geotechnical and Geological Engineering*, 24(3), 523–549. doi:10.1007/s10706-004-5832-6.
- [66] Won, M. S., Langcuyan, C. P., & Choi, G. H. (2021). Experimental study on the behavior of MSE wall having full-height rigid facing and segmental panel-type wall facing. *Open Geosciences*, 13(1), 932–943. doi:10.1515/geo-2020-0278.
- [67] Hamidi, A., Alizadeh, M., & Soleimani, S. M. (2009). Effect of particle crushing on shear strength and dilation characteristics of sand-gravel mixtures. *International Journal of Civil Engineering*, 7(1), 61–71.
- [68] Strahler, A., Stuedlein, A. W., & Arduino, P. W. (2016). Stress-Strain Response and Dilatancy of Sandy Gravel in Triaxial Compression and Plane Strain. *Journal of Geotechnical and Geoenvironmental Engineering*, 142(4). doi:10.1061/(asce)gt.1943-5606.0001435.
- [69] Stacho, J., Sulovska, M., & Hrustinec, L. (2024). Determining the Dilatancy of Gravels Using a Large-size Direct Shear Test. *Jordan Journal of Civil Engineering*, 18(3), 492–502. doi:10.14525/JJCE.v18i3.11.
- [70] Michalowski, R. L., & Čermák, J. (2003). Triaxial Compression of Sand Reinforced with Fibers. *Journal of Geotechnical and Geoenvironmental Engineering*, 129(2), 125–136. doi:10.1061/(asce)1090-0241(2003)129:2(125).
- [71] Gray, D. H., & Ohashi, H. (1983). Mechanics of fiber reinforcement in sand. *Journal of Geotechnical Engineering*, 109(3), 335–353. doi:10.1061/(ASCE)0733-9410(1983)109:3(335).